



Stress-driven Approach to Vibrational Analysis of FGM Annular Nano-plate based on First-order Shear Deformation Plate Theory

Mojtaba Shariati¹, Mohammad Shishehsaz², Reza Mosalmani³

¹ Department of Mechanical Engineering, Shahid Chamran University of Ahvaz, Ahvaz, Iran, Email: mojtaba.shariati456@gmail.com

² Department of Mechanical Engineering, Shahid Chamran University of Ahvaz, Ahvaz, Iran, Email: mshishehsaz@scu.ac.ir

³ Department of Mechanical Engineering, Shahid Chamran University of Ahvaz, Ahvaz, Iran, Email: mosalmani@scu.ac.ir

Received June 16 2022; Revised August 18 2022; Accepted for publication August 18 2022.

Corresponding author: M. Shishehsaz (mshishehsaz@scu.ac.ir)

© 2022 Published by Shahid Chamran University of Ahvaz

Abstract. Vibrational behavior of small-scale functionally graded annular plate based on the first-order shear deformation theory, and non-local stress-driven model is investigated. For the first time, generalized differential quadrature rule is utilized to solve the governing equation and related boundary conditions. The convergence, accuracy, and efficiency of the generalized differential quadrature rule are investigated using problem-solving for different situations. The effects of parameters such as size parameter, inhomogeneity coefficient of functionally graded materials, thickness to outer radius ratio, inner radius to outer radius ratio, and boundary conditions on the natural frequency of the structure have been investigated. Results show that, unlike the strain-driven model, the non-local stress-driven theory predicts the same behavior for all boundary conditions and increasing the size parameter has led to a stiffening behavior and an increase in the natural frequency of the structure.

Keywords: Size effect, vibrational response, functionally graded material, circular nanoplate, First-order Shear deformation plate theory.

1. Introduction

The tendency of humans to use tools to make things easier has led to the use of materials with new properties. Some materials produced by scientists and even some materials found in nature have extraordinary properties. The use of functionally grade materials (FGM) in nano-dimensions has greatly helped to build accurate and important tools in industry and medicine. They have many applications in drug delivery [1-3], reducing the size of computer chips [4-6], elimination of pollutants [7, 8], high energy density batteries [9, 10], high-sensitivity sensors [11, 12], longer-lasting medical implants [13, 14], aerospace components with enhanced performance characteristics [15-18], etc. For example, a US nanotechnology company has developed contact lenses that can be used instead of large virtual reality headsets without affecting the individual's vision. In another example, nano-sensors are built to detect a heart attack and nano-materials have been discovered to prevent the spread of bacteria. These important properties have prompted engineers to research new materials, including nano-materials.

As mentioned, the properties of materials in very small dimensions (nano) are different from the properties of the same materials in large dimensions and this difference has led to the introduction of new theories about the behavior of nano-materials. Examining the properties of materials in a laboratory is very difficult and expensive [19-21]. Also, using the molecular dynamics method to study the behavior of materials in the nano-scale has a high computational cost [22-25]. Therefore, the best way to study materials in nano-dimensions is to use non-classical mechanical continuum approaches. Theories related to nano-materials are more complex than classical theories. Some of the theories developed in relation to nano-materials are nonlocal elasticity theory [26-30], strain gradient theory [31-37], surface effect theory [38-45], couple stress theory [46-52], doublet mechanics [53-55] and etc.

Romano and Barretta [56] proposed a new classification of nonlocal elasticity. Regarding this classification, there are two different definitions of fully nonlocal integral elasticity. The first is a strain-driven nonlocal integral model which was adopted by Eringen [57, 58], and stress-driven nonlocal integral model. In the first model, the nonlocal stress is defined by an integral convolution of elastic strain with an averaging kernel dependent on a nonlocal parameter. Strain-driven could be applied to many nano-structural problems with unbounded domains that the involved fields that vanish at infinity. This is one of the most well-known modified continuum mechanics theories that includes small scale effects that are used by many researchers to simulate the nonlocality of nano-structure in the last decade [59-61]. Furthermore, this was replaced with an equivalent differential equation under boundary conditions that vanish at infinity. This equivalent form was later utilized to simulate and analyze the mechanical characteristics of nanoscopic structures over bounded continuous domains. A comprehensive review on the application of the nonlocal differential-based models for modeling size-effects in nano-structures can be found in Rafii-Tabar *et al.*



[62]. However, Romano et al. [63] showed that, when suitable constitutive boundary conditions are added for bounded domains then the integral convolutions can be replaced with differential relations. Additionally, the associated elastic problems are ill-posed when the constitutive boundary conditions are incompatible with equilibrium conditions. Another point is emerging serious difficulties and undesirable results. On the other hand, Romano and Barretta [56] showed that, in the stress-driven nonlocal integral model, the nonlocal elastic strain is defined by an integral convolution of stress with an averaging kernel dependent on a nonlocal parameter. They showed that, this model is well-posed for structures defined on bounded domains and suffers from no inconsistencies. This approach was applied to several static and dynamic problems of the nano-structures [64-70]. In contrast to the strain-driven nonlocal models, the results calculated from the stress-driven model exhibit a hardening behavior when nonlocality is increasing and have been confirmed by Shariati et al. [71].

Shishehsaz et al. [72] and Shariati et al. [73] analyzed the vibrational behavior of functionally graded size-dependent circular and annular nano-plates using the stress-driven nonlocal integral elasticity as well as the strain gradient theory in conjunction with the classical plate theory. They studied the influences of various parameters such as the size-effect parameter, material heterogeneity index, the aspect ratio of the inner to outer radii, and the effects of different boundary conditions on the vibrational behavior of the nano-plate, based on different types of boundary conditions. They indicated that the natural frequencies of the FGM nanoplate increase with an increase in the heterogeneity index n and the increase in size-effect parameter show a similar effect in both models. An important question that arises from previous studies is; Can the non-local model be used for any geometry, inhomogeneity coefficient and size parameter according to the efficiency of the stress-driven model based on the classical plate theory? Or the stress-driven model based on the first-order shear deformation theory should be used? To answer this important question, first, the governing equations of the structure were obtained in the framework of the non-local stress-driven model based on the first-order shear deformation theory. Then, using the generalized differential quadrature rule (GDQR) numerical solution, the natural frequency of the structure with different boundary conditions for the mentioned parameters was calculated and compared with the results of non-local stress-driven model based on the classical plate theory. As it is known, when the ratio $h/(b-a)$ is less than 0.2, the FSDT can be used to obtain natural frequencies (b and a are the outside and inside radiuses of the annular plate, respectively). Regarding this, the aspect ratios a/b and h/b are chosen in such a way that with the ratio $h/(b-a)$ is less than 0.2.

Therefore, for the first time, the vibration behavior of functionally graded annular plates was analyzed using combination of the first-order shear deformation plate theory, and non-local stress-driven model. The convergence, accuracy, and efficiency of the GDQR are shown by various examples. Limited research on nanoplates has been done using this method, while much more research has been done on beams. It should also be noted that most researchers have used the generalized differential quadrature method (GDQ) to solve the equations, while in this study the generalized differential quadrature rule (GDQR) has been used.

2. FGM Annular Nano-plate

An annular nano-plate of thickness h , inner and outer radii a and b is shown in Fig. 1. To obtain the equations of motion and study the vibrational response of the small-scale annular nano-plate based on Mindlin plate theory and stress-driven nonlocal integral elasticity, an axisymmetric cylindrical coordinate system (r, z) is used.

Ceramic and metal are the selected material used for the FGM nano-plate and the material properties, Young's modulus E and the mass density ρ were assumed to vary along the thickness according to Eq. (1). Additionally, it is assumed that the Poisson's ratio ν is constant in the thickness direction.

$$E(r, z, t) = E_c V^n + E_m (1 - V^n), \quad \rho(r, z, t) = \rho_c V^n + \rho_m (1 - V^n). \quad (1)$$

where n is a gradient index and the subscripts m and c refer to the metal and ceramic constituents, respectively. Also, V is the volume fraction of the ceramic material, and it is assumed such as:

$$V = \frac{2z+h}{2h}, \quad -\frac{h}{2} \leq z \leq +\frac{h}{2} \quad (2)$$

3. First-order Shear Deformation Plate Theory based on the Local Elasticity

Based on the first-order shear deformation plate theory (FSDT), the component of displacement field u_r and u_z in the radial and transverse directions, respectively, are assumed to vary as follows [74]:

$$u_r(r, z, t) = u_0(r, t) + z\phi(r, t), \quad u_z(r, z, t) = w_0(r, t). \quad (3)$$

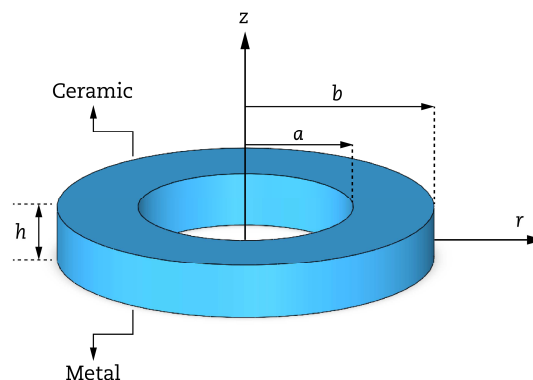


Fig. 1. Configuration of an annular nano-plate and coordinate system.



where u_0 and w_0 are the displacement components of the mid-plane surface in the radial and transverse directions. Also, ϕ is angular rotation of the normal to the middle surface in radial direction [75]. Also, the non-zero strain component, based on the strain-displacement relationship, is given by [74]:

$$\epsilon_{rr} = \frac{\partial u_r}{\partial r} = \frac{\partial u_0}{\partial r} + z \frac{\partial \phi}{\partial r} = \epsilon_{rr}^0 + z \kappa_{rr}, \quad \epsilon_{\theta\theta} = \frac{u_r}{r} = \frac{u_0}{r} + z \frac{1}{r} \phi = \epsilon_{\theta\theta}^0 + z \kappa_{\theta\theta}, \quad \gamma_{rz} = \frac{\partial u_r}{\partial z} + \frac{\partial u_z}{\partial r} = \frac{\partial w_0}{\partial r} + \phi. \tag{4}$$

where ϵ_{rr}^0 and $\epsilon_{\theta\theta}^0$ are the normal radial and hoop local elastic strains associated with the mid-plane surface. Also, κ_{rr} and $\kappa_{\theta\theta}$ are the principal curvatures of the deflected surface and γ_{rz} is out of plane shear strain.

Using Hamilton's principle, the equations of motion and boundary conditions of annular plate based on the FSDT are derived such as [74]:

$$\begin{aligned} \frac{\partial N_{rr}}{\partial r} + \frac{1}{r} N_{rr} - \frac{1}{r} N_{\theta\theta} &= I_0 \frac{\partial^2 u_0}{\partial t^2} - I_1 \frac{\partial^2 \phi}{\partial t^2}, \\ \frac{\partial Q_r}{\partial r} + \frac{1}{r} Q_r &= I_0 \frac{\partial^2 w_0}{\partial t^2}, \\ \frac{\partial M_{rr}}{\partial r} + \frac{1}{r} M_{rr} - \frac{1}{r} M_{\theta\theta} + Q_r &= -I_1 \frac{\partial^2 u_0}{\partial t^2} + I_2 \frac{\partial^2 \phi}{\partial t^2}. \end{aligned} \tag{5}$$

$$\begin{aligned} (1) \quad N_{rr} = 0 \quad \text{or} \quad u_0 = 0 \quad (2) \quad Q_r = 0 \quad \text{or} \quad w_0 = 0 \\ (3) \quad M_{rr} = 0 \quad \text{or} \quad \phi = 0 \end{aligned} \tag{6}$$

where, the stress resultants N_{rr} , $N_{\theta\theta}$, Q_r , M_{rr} and $M_{\theta\theta}$, as well as the mass moments of inertias I_0 , I_1 , and I_2 are defined as:

$$\begin{aligned} (N_{rr}, N_{\theta\theta}, Q_r, M_{rr}, M_{\theta\theta}) &= \int_{-\frac{h}{2}}^{+\frac{h}{2}} (\sigma_{rr}, \sigma_{\theta\theta}, \tau_{rz}, z\sigma_{rr}, z\sigma_{\theta\theta}) dz, \\ (I_0, I_1, I_2) &= \int_{-\frac{h}{2}}^{+\frac{h}{2}} (1, z, z^2) \rho dz. \end{aligned} \tag{7}$$

4. FSDT based on Nonlocal Elasticity, Stress-driven Model

Based on the FSDT, the components of strain tensor can be written such as:

$$\epsilon_{rr} = \frac{1}{E} (\sigma_{rr} - \nu \sigma_{\theta\theta}), \quad \epsilon_{\theta\theta} = \frac{1}{E} (-\nu \sigma_{rr} + \sigma_{\theta\theta}), \quad \gamma_{rz} = \frac{2(1+\nu)}{E} \tau_{rz}. \tag{8}$$

using Eq. (7) and Eq. (8) leads to:

$$A \begin{Bmatrix} \epsilon_{rr}^0 \\ \epsilon_{\theta\theta}^0 \end{Bmatrix} + B \begin{Bmatrix} \kappa_{rr} \\ \kappa_{\theta\theta} \end{Bmatrix} = \begin{bmatrix} 1 & -\nu \\ -\nu & 1 \end{bmatrix} \begin{Bmatrix} N_{rr} \\ N_{\theta\theta} \end{Bmatrix}, \quad B \begin{Bmatrix} \epsilon_{rr}^0 \\ \epsilon_{\theta\theta}^0 \end{Bmatrix} + D \begin{Bmatrix} \kappa_{rr} \\ \kappa_{\theta\theta} \end{Bmatrix} = \begin{bmatrix} 1 & -\nu \\ -\nu & 1 \end{bmatrix} \begin{Bmatrix} M_{rr} \\ M_{\theta\theta} \end{Bmatrix}, \quad \gamma_{rz} = \frac{1}{C} Q_r. \tag{9}$$

where A, B, C, and D are the stiffness coefficients and defined as follows:

$$(A, B, C, D) = \int_{-h/2}^{+h/2} E(z) \left(1, z, \frac{k}{2(1+\nu)}, z^2 \right) dz \tag{10}$$

Finally, the mid-plane surface strain, ϵ_{rr}^0 and $\epsilon_{\theta\theta}^0$, the curvature, κ_{rr} and $\kappa_{\theta\theta}$, and the out of plane shear strain, γ_{rz} , can be obtained by using Eq. (9) such as:

$$\begin{aligned} \epsilon_{rr}^0 &= \frac{D}{AD - B^2} (N_{rr} - \nu N_{\theta\theta}) - \frac{B}{AD - B^2} (M_{rr} - \nu M_{\theta\theta}), \\ \epsilon_{\theta\theta}^0 &= \frac{D}{AD - B^2} (N_{\theta\theta} - \nu N_{rr}) - \frac{B}{AD - B^2} (M_{\theta\theta} - \nu M_{rr}), \quad \gamma_{rz} = \frac{Q_r}{C}, \\ \kappa_{rr} &= \frac{-B}{AD - B^2} (N_{rr} - \nu N_{\theta\theta}) + \frac{A}{AD - B^2} (M_{rr} - \nu M_{\theta\theta}), \\ \kappa_{\theta\theta} &= \frac{-B}{AD - B^2} (N_{\theta\theta} - \nu N_{rr}) + \frac{A}{AD - B^2} (M_{\theta\theta} - \nu M_{rr}). \end{aligned} \tag{11}$$

The stress-driven model (SDM) proposed by Romano and Barretta [56] for nano-beams, is used to capture the size effects in axisymmetric vibrational behavior of annular nano-plates based on classical plate theory [76]. In this section based on SDM and first-order shear deformation theory by assuming the non-local elasticity for the radial strain of the mid-plane surface, ϵ_{rr}^0 , radial curvature κ_{rr} , and the out of plane shear strain, γ_{rz} , it can be written;

$$\begin{aligned} \epsilon_{rr}^0 &= \int_a^b \varphi_L \left\{ \frac{D}{AD - B^2} (N_{rr} - \nu N_{\theta\theta}) - \frac{B}{AD - B^2} (M_{rr} - \nu M_{\theta\theta}) \right\} d\rho, \\ \kappa_{rr} &= \int_a^b \varphi_L \left\{ \frac{-B}{AD - B^2} (N_{rr} - \nu N_{\theta\theta}) + \frac{A}{AD - B^2} (M_{rr} - \nu M_{\theta\theta}) \right\} d\rho, \quad \gamma_{rz} = \int_a^b \varphi_L \left\{ \frac{Q_r}{C} \right\} d\rho. \end{aligned} \tag{12}$$

where φ_L is the averaging kernel with the following properties:



$$\varphi_L(r) \geq 0, \quad \int_{-\infty}^{+\infty} \varphi_L(r) dr = 1, \quad \lim_{L \rightarrow 0^+} \int_{-\infty}^{+\infty} \varphi_L(r - \rho) f(r) dr = f(\rho). \tag{13}$$

and L is the characteristic length that can describe the size effects. In Eq. (13), f is any continuous test field [76]. In this study, exponential kernel function used for the analysis is expressed by Eq. (14). It can be proven that the following function fulfils all the necessary properties given by the set of Eq. (13):

$$\varphi_L(r) = \frac{1}{2L} \exp\left(-\frac{|r|}{L}\right) \tag{14}$$

Using Eq. (14), Eq. (12) can be converted to the following stress-driven nonlocal differential equations, Eq. (15), with the constitutive boundary conditions in Eq. (16) as:

$$\begin{aligned} \varepsilon_{rr}^0 - L^2 \frac{\partial^2}{\partial r^2} \varepsilon_{rr}^0 &= \frac{D}{AD - B^2} (N_{rr} - \nu N_{\theta\theta}) - \frac{B}{AD - B^2} (M_{rr} - \nu M_{\theta\theta}), \\ \kappa_{rr} - L^2 \frac{\partial^2}{\partial r^2} \kappa_{rr} &= \frac{-B}{AD - B^2} (N_{rr} - \nu N_{\theta\theta}) + \frac{A}{AD - B^2} (M_{rr} - \nu M_{\theta\theta}), \quad \gamma_{rz} - L^2 \frac{\partial^2}{\partial r^2} \gamma_{rz} = \frac{Q_r}{C}. \end{aligned} \tag{15}$$

$$\begin{aligned} @ r = a : \quad \frac{\partial \varepsilon_{rr}^0}{\partial r} - \frac{1}{L} \varepsilon_{rr}^0 &= 0, \quad \frac{\partial \kappa_{rr}}{\partial r} - \frac{1}{L} \kappa_{rr} = 0, \quad \frac{\partial \gamma_{rz}}{\partial r} - \frac{1}{L} \gamma_{rz} = 0. \\ @ r = b : \quad \frac{\partial \varepsilon_{rr}^0}{\partial r} + \frac{1}{L} \varepsilon_{rr}^0 &= 0, \quad \frac{\partial \kappa_{rr}}{\partial r} + \frac{1}{L} \kappa_{rr} = 0, \quad \frac{\partial \gamma_{rz}}{\partial r} + \frac{1}{L} \gamma_{rz} = 0. \end{aligned} \tag{16}$$

using Eq. (4) into Eq. (15), the stress resultants can be obtained such as Eq. (17):

$$\begin{aligned} \{N_{rr}, M_{rr}\} &= \frac{\{A, B\}}{1 - \nu^2} \frac{A}{1 - \nu^2} \left(\frac{\partial u_0}{\partial r} + \nu \frac{u_0}{r} - L^2 \frac{\partial^3 u_0}{\partial r^3} \right) + \frac{B}{1 - \nu^2} \left(\frac{\partial \phi}{\partial r} + \nu \frac{1}{r} \phi - L^2 \frac{\partial^3 \phi}{\partial r^3} \right), \\ \{N_{\theta\theta}, M_{\theta\theta}\} &= \frac{\{A, B\}}{1 - \nu^2} \frac{A}{1 - \nu^2} \left(\nu \frac{\partial u_0}{\partial r} + \frac{u_0}{r} - \nu L^2 \frac{\partial^3 u_0}{\partial r^3} \right) + \frac{B}{1 - \nu^2} \left(\nu \frac{\partial \phi}{\partial r} + \frac{1}{r} \phi - \nu L^2 \frac{\partial^3 \phi}{\partial r^3} \right), \\ Q_r &= C \left(\frac{\partial w_0}{\partial r} + \phi - L^2 \frac{\partial^2}{\partial r^2} \left(\frac{\partial w_0}{\partial r} + \phi \right) \right). \end{aligned} \tag{17}$$

The equations of motion for the annular nano-plate based on the SDM and FSDT can be obtained by substituting Eq. (17) into Eq. (5) such as:

$$\begin{aligned} A \left(\left[\frac{\partial^2 u_0}{\partial r^2} + \frac{1}{r} \frac{\partial u_0}{\partial r} - \frac{1}{r^2} u_0 \right] - L^2 \left[\frac{\partial^4 u_0}{\partial r^4} - \frac{\nu - 1}{r} \frac{\partial^3 u_0}{\partial r^3} \right] \right) \\ - B \left(\left[\frac{\partial^2 \phi}{\partial r^2} + \frac{1}{r} \frac{\partial \phi}{\partial r} - \frac{1}{r^2} \phi \right] - L^2 \left[\frac{\partial^4 \phi}{\partial r^4} - \frac{\nu - 1}{r} \frac{\partial^3 \phi}{\partial r^3} \right] \right) &= (1 - \nu^2) \left(I_0 \frac{\partial^2 u_0}{\partial t^2} - I_1 \frac{\partial^2 \phi}{\partial t^2} \right), \\ C \left(\left[\frac{\partial^2 w_0}{\partial r^2} + \frac{1}{r} \frac{\partial w_0}{\partial r} + \frac{\partial \phi}{\partial r} + \frac{1}{r} \phi \right] - L^2 \left[\frac{\partial^4 w_0}{\partial r^4} + \frac{1}{r} \frac{\partial^3 w_0}{\partial r^3} + \frac{\partial^3 \phi}{\partial r^3} + \frac{1}{r} \frac{\partial^2 \phi}{\partial r^2} \right] \right) &= I_0 (1 - \nu^2) \frac{\partial^2 w_0}{\partial t^2}, \\ B \left(\left[\frac{\partial^2 u_0}{\partial r^2} + \frac{1}{r} \frac{\partial u_0}{\partial r} - \frac{1}{r^2} u_0 \right] - L^2 \left[\frac{\partial^4 u_0}{\partial r^4} - \frac{\nu - 1}{r} \frac{\partial^3 u_0}{\partial r^3} \right] \right) - C \left(\left[\frac{\partial w_0}{\partial r} + \phi \right] - L^2 \left[\frac{\partial^3 w_0}{\partial r^3} + \frac{\partial^2 \phi}{\partial r^2} \right] \right) \\ + D \left(\left[\frac{\partial^2 \phi}{\partial r^2} + \frac{1}{r} \frac{\partial \phi}{\partial r} - \frac{\phi}{r^2} \right] - L^2 \left[\frac{\partial^4 \phi}{\partial r^4} - \frac{\nu - 1}{r} \frac{\partial^3 \phi}{\partial r^3} \right] \right) &= (1 - \nu^2) \left(I_2 \frac{\partial^2 \phi}{\partial t^2} - I_1 \frac{\partial^2 u_0}{\partial t^2} \right). \end{aligned} \tag{18}$$

Also, substituting Eq. (4) into the Eq. (16), the constitutive boundary condition can be obtained as follows by:

$$\begin{aligned} @ r = a : \quad \begin{cases} \frac{\partial^2 u_0}{\partial r^2} - \frac{1}{L} \frac{\partial u_0}{\partial r} = 0, \quad \frac{\partial^2 \phi}{\partial r^2} - \frac{1}{L} \frac{\partial \phi}{\partial r} = 0 \\ \left(\frac{\partial^2 w_0}{\partial r^2} + \frac{\partial \phi}{\partial r} \right) - \frac{1}{L} \left(\frac{\partial w_0}{\partial r} + \phi \right) = 0 \end{cases}, \\ @ r = b : \quad \begin{cases} \frac{\partial^2 u_0}{\partial r^2} + \frac{1}{L} \frac{\partial u_0}{\partial r} = 0, \quad \frac{\partial^2 \phi}{\partial r^2} + \frac{1}{L} \frac{\partial \phi}{\partial r} = 0 \\ \left(\frac{\partial^2 w_0}{\partial r^2} + \frac{\partial \phi}{\partial r} \right) + \frac{1}{L} \left(\frac{\partial w_0}{\partial r} + \phi \right) = 0 \end{cases}. \end{aligned} \tag{19}$$

It can be concluded that by setting the parameter L equal to zero in Eq. (18), the equation of motion for the annular plate based on the local FSDT can be achieved.

The different states of the possible boundary conditions for the annular plate are shown in Figs. (2-5).

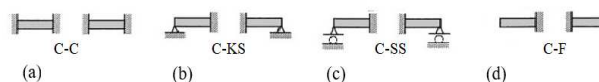


Fig. 2. Clamped inner condition and (a) clamped, (b) knifed support, (c) simply support, and (d) free outer.



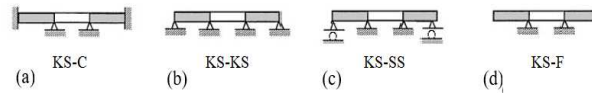


Fig. 3. Knifed support inner edge and (a) clamped, (b) knifed support, (c) simply supported, and (d) free outer.

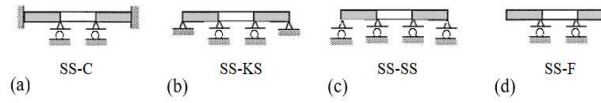


Fig. 4. Simply inner edge and (a) clamped, (b) knifed support, (c) simply support, and (d) free outer edges.

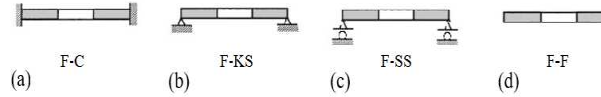


Fig. 5. Free inner edge and (a) clamped, (b) knifed support, (c) simply support, and (d) free outer edges.

The boundary condition can be obtained by using Eq. (6) and Eq. (17). The associated mathematical relations are given in Table 1. Using the oscillating response assumption, the appropriate solutions for $u_0(r,t)$, $w_0(r,t)$ and $\phi(r,t)$ can be obtained such as:

$$\{ u_0(r,t) , w_0(r,t) , \phi(r,t) \} = \{ u(r) , w(r) , \phi(r) \} e^{i\omega_n t} \tag{20}$$

where the natural frequency of the annular nano-plate is ω_n . Also, to analyze the influence of effective parameters on the natural frequencies of the FGM annular plate, the non-dimensional variables are defined such as Eq. (21):

$$\begin{aligned} (s,U,W,\alpha,\bar{h},L_c) &= \frac{1}{b}(r,u,w,a,h,L), \quad \Phi = \phi, \\ (\bar{A},\bar{B},\bar{C},\bar{D}) &= \left(\frac{Ab^2}{D_0}, \frac{Bb}{D_0}, \frac{Cb^2}{D_0}, \frac{D}{D_0} \right), \quad (\bar{I}_0, \bar{I}_1, \bar{I}_2) = \left(\frac{I_0}{I_{00}}, \frac{I_1}{I_{00}b}, \frac{I_2}{I_{00}b^2} \right), \\ \Omega_n^2 &= \frac{I_{00}b^4}{D_0}\omega_n^2, \quad D_0 = \frac{E_m h^3}{12(1-\nu^2)}, \quad I_{00} = \rho_m h. \end{aligned} \tag{21}$$

The non-dimensional governing equations and the corresponding constitutive boundary conditions can be obtained by substituting Eq. (21) into Eq. (18-19), as follows:

$$\begin{aligned} \bar{A} \left(\frac{d^2U}{ds^2} + \frac{1}{s} \frac{dU}{ds} - \frac{1}{s^2} U \right) - L_c^2 \left(\frac{d^4U}{dr^4} - \frac{\nu-1}{r} \frac{d^3U}{dr^3} \right) - \bar{B} \left(\frac{d^2\Phi}{ds^2} + \frac{1}{s} \frac{d\Phi}{ds} - \frac{1}{s^2} \Phi \right) - L_c^2 \left(\frac{d^4\Phi}{ds^4} - \frac{\nu-1}{s} \frac{d^3\Phi}{ds^3} \right) &= \{ \bar{I}_1\Phi - \bar{I}_0U \} \Omega_n^2, \\ \bar{C} \left(\frac{d^2W}{ds^2} + \frac{1}{s} \frac{dW}{ds} - \frac{d\Phi}{ds} - \frac{1}{s} \Phi \right) - L_c^2 \left(\frac{d^4W}{ds^4} + \frac{1}{s} \frac{d^3W}{ds^3} - \frac{d^3\Phi}{ds^3} - \frac{1}{s} \frac{d^2\Phi}{ds^2} \right) &= -\bar{I}_0W\Omega_n^2, \\ \bar{B} \left(\frac{d^2U}{ds^2} + \frac{1}{s} \frac{dU}{ds} - \frac{1}{s^2} U \right) - L_c^2 \left(\frac{d^4U}{ds^4} - \frac{\nu-1}{s} \frac{d^3U}{ds^3} \right) + \bar{D} \left(\frac{d^2\Phi}{ds^2} + \frac{1}{s} \frac{d\Phi}{ds} - \frac{\Phi}{s^2} \right) - L_c^2 \left(\frac{d^4\Phi}{ds^4} - \frac{\nu-1}{s} \frac{d^3\Phi}{ds^3} \right) - \bar{C} \left(\frac{dW}{dr} + \Phi \right) - L_c^2 \left(\frac{d^3W}{ds^3} + \frac{d^2\Phi}{ds^2} \right) &= \{ \bar{I}_1U - \bar{I}_2\Phi \} \Omega_n^2. \end{aligned} \tag{22}$$

$$\begin{aligned} @s=1: \left\{ \begin{aligned} \frac{d^2U}{ds^2} - \frac{1}{L_c} \frac{dU}{ds} = 0, \quad \frac{d^2\Phi}{ds^2} - \frac{1}{L_c} \frac{d\Phi}{ds} = 0, \\ \left(\frac{d^2W}{ds^2} - \frac{d\Phi}{ds} \right) - \frac{1}{L_c} \left(\frac{dW}{ds} - \Phi \right) = 0 \end{aligned} \right. , @s=\alpha: \left\{ \begin{aligned} \frac{d^2U}{ds^2} + \frac{1}{L_c} \frac{dU}{ds} = 0, \quad \frac{d^2\Phi}{ds^2} + \frac{1}{L_c} \frac{d\Phi}{ds} = 0, \\ \left(\frac{d^2W}{ds^2} - \frac{d\Phi}{ds} \right) + \frac{1}{L_c} \left(\frac{dW}{ds} - \Phi \right) = 0 \end{aligned} \right. \end{aligned} \tag{23}$$

Also, on using Eq. (21), the boundary condition in Table 1 can be recast in a non-dimensional form as given in Table 2.

Table 1. Boundary condition and mathematical relation of annular plate based on SDM and FSDT.

Boundary condition	Associated mathematical relations
Clamped	$u_0 = w_0 = \phi = 0$
Knifed support	$u_0 = w_0 = 0, \quad M_{rr} = 0 \Rightarrow B \left(\frac{\partial u_0}{\partial r} + \nu \frac{u_0}{r} - L^2 \frac{\partial^3 u_0}{\partial r^3} \right) + D \left(\frac{\partial \phi}{\partial r} + \nu \frac{1}{r} \phi - L^2 \frac{\partial^3 \phi}{\partial r^3} \right) = 0.$
Simply supported	$w_0 = 0, \quad \{N_r, M_{rr}\} = 0 \Rightarrow \{A, B\} \left(\frac{\partial u_0}{\partial r} + \nu \frac{u_0}{r} - L^2 \frac{\partial^3 u_0}{\partial r^3} \right) + \{B, D\} \left(\frac{\partial \phi}{\partial r} + \nu \frac{1}{r} \phi - L^2 \frac{\partial^3 \phi}{\partial r^3} \right) = 0.$
Free	$Q_r = 0 \Rightarrow C \left(\frac{\partial w_0}{\partial r} + \phi \right) - L^2 \left(\frac{\partial^2 w_0}{\partial r^2} + \frac{\partial^2 \phi}{\partial r^2} \right) = 0,$ $\{N_r, M_{rr}\} = 0 \Rightarrow \{A, B\} \left(\frac{\partial u_0}{\partial r} + \nu \frac{u_0}{r} - L^2 \frac{\partial^3 u_0}{\partial r^3} \right) + \{B, D\} \left(\frac{\partial \phi}{\partial r} + \nu \frac{1}{r} \phi - L^2 \frac{\partial^3 \phi}{\partial r^3} \right) = 0.$



Table 2. The non-dimensional mathematical relations based on the possible boundary conditions for the annular plate in question.

Boundary condition	Associated mathematical relations
Clamped	$U = W = \Phi = 0$
Knifed support	$U = W = 0, \quad \bar{B} \left(\frac{dU}{ds} + \nu \frac{U}{s} - L_c^2 \frac{d^3U}{ds^3} \right) + \bar{D} \left(\frac{d\Phi}{ds} + \nu \frac{1}{s} \Phi - L_c^2 \frac{d^3\Phi}{ds^3} \right) = 0.$
Simply supported	$W = 0, \quad \{ \bar{A}, \bar{B} \} \left(\frac{dU}{ds} + \nu \frac{U}{s} - L_c^2 \frac{d^3U}{ds^3} \right) + \{ \bar{B}, \bar{D} \} \left(\frac{d\Phi}{ds} + \nu \frac{1}{s} \Phi - L_c^2 \frac{d^3\Phi}{ds^3} \right) = 0.$
Free	$\left(\frac{dW}{ds} + \Phi \right) - L_c^2 \left(\frac{d^3W}{ds^3} + \frac{d^2\Phi}{ds^2} \right) = 0,$ $\{ \bar{A}, \bar{B} \} \left(\frac{dU}{ds} + \nu \frac{U}{s} - L_c^2 \frac{d^3U}{ds^3} \right) + \{ \bar{B}, \bar{D} \} \left(\frac{d\Phi}{ds} + \nu \frac{1}{s} \Phi - L_c^2 \frac{d^3\Phi}{ds^3} \right) = 0.$

5. Method of Solution

The high-order differential equations related to Euler beam and plate fourth-order differential equations have been solved using the generalized differential quadrature rule (GDQR) [77] as a general numerical method. In the present study, the free vibration of the FGM annular nano-plate based on the stress-driven model and Mindlin’s plate theory is governed by a system of fourth-order differential equations, which is constrained by six boundary conditions on each edge.

Based on GDQR method, the n^{th} order derivatives of functions $U(s)$, $W(s)$, and $\Phi(s)$ at any discrete point of a domain are approximated by a weighted linear sum of the function values at all discrete points $s = s_i$ ($i=1, 2, \dots, N$) [77] such that:

$$\{U^{(n)}, W^{(n)}, \Phi^{(n)}\}(s_i) = \sum_{k=0}^1 h_{1k}^{(n)}(s_i) \{U_1^{(k)}, W_1^{(k)}, \Phi_1^{(k)}\} + \sum_{j=2}^{N-1} h_{j0}^{(n)}(s_i) \{U_j^{(k)}, W_j^{(k)}, \Phi_j^{(k)}\} + \sum_{k=0}^1 h_{Nk}^{(n)}(s_i) \{U_N^{(k)}, W_N^{(k)}, \Phi_N^{(k)}\} = \sum_{k=1}^{N+2} E_{ik}^{(n)} \{ \Psi_k, \Theta_k, \Upsilon_k \} \tag{24}$$

where,

$$\begin{aligned} \{E_{ik}^{(n)}\}^T &= \{h_{10}^{(n)}(s_i), h_{11}^{(n)}(s_i), h_{20}^{(n)}(s_i), \dots, h_{(N-1)0}^{(n)}(s_i), h_{N0}^{(n)}(s_i), h_{N1}^{(n)}(s_i)\} \\ \{\Psi_1, \Psi_2, \dots, \Psi_j, \dots, \Psi_{N+2}\} &= \{U_1, U_1^{(1)}, U_2, \dots, U_N, U_N^{(1)}\}, \\ \{\Theta_1, \Theta_2, \dots, \Theta_j, \dots, \Theta_{N+2}\} &= \{W_1, W_1^{(1)}, W_2, \dots, W_N, W_N^{(1)}\}, \\ \{\Upsilon_1, \Upsilon_2, \dots, \Upsilon_j, \dots, \Upsilon_{N+2}\} &= \{\Phi_1, \Phi_1^{(1)}, \Phi_2, \dots, \Phi_N, \Phi_N^{(1)}\}, \quad s_i = \frac{1}{2} \left(1 - \cos \left(\frac{i-1}{N-1} \pi \right) \right). \end{aligned} \tag{25}$$

and the weighting coefficients in Eq. (24-25) are defined as follows:

$$\begin{aligned} h_{ki}(x) &= (a_{ki}x^2 + b_{ki}x + c_{ki})L_1(x) \quad (i = 0, 1), (k = 1, N) \\ h_{j0}(x) &= \frac{(x - x_1)(x - x_N)}{(x_j - x_1)(x_j - x_N)}L_j(x) \quad (j = 2, 3, \dots, N - 1) \end{aligned}$$

$$\begin{cases} a_{10} = \frac{-1}{(x_1 - x_N)^2} - \frac{L_1^{(1)}(x_1)}{(x_1 - x_N)}, \quad b_{10} = \frac{1}{(x_1 - x_N)} - a_{10}(x_1 + x_N), \quad c_{10} = 1 - a_{10}x_1^2 - b_{10}x_1, \\ a_{11} = \frac{1}{(x_1 - x_N)}, \quad b_{10} = -\frac{(x_1 + x_N)}{(x_1 - x_N)}, \quad c_{10} = \frac{x_1x_N}{(x_1 - x_N)}. \\ a_{N0} = \frac{-1}{(x_1 - x_N)^2} + \frac{L_1^{(N)}(x_N)}{(x_1 - x_N)}, \quad b_{N0} = \frac{-1}{(x_1 - x_N)} - a_{N0}(x_1 + x_N), \quad c_{N0} = 1 - a_{N0}x_N^2 - b_{N0}x_N, \\ a_{N1} = \frac{-1}{(x_1 - x_N)}, \quad b_{N0} = \frac{(x_1 + x_N)}{(x_1 - x_N)}, \quad c_{N0} = \frac{-x_1x_N}{(x_1 - x_N)}. \end{cases} \tag{26}$$

where $L(x)$ is a Lagrange interpolation function with the following properties [77]:

$$L_i(x_j) = \begin{cases} 1 & i=j \\ 0 & i \neq j \end{cases} \tag{27}$$

and the first and second derivatives of the Lagrange interpolation function have been explicitly obtained in [78, 79].

The equation of motion and the constitutive boundary conditions, Eq. (21-22) can be written into the following form by using Eq. (23):

$$\begin{aligned} \bar{A} \left(\left\{ \sum_{k=1}^{N+2} E_{ik}^{(2)} \Psi_k + \frac{1}{s} \sum_{k=1}^{N+2} E_{ik}^{(1)} \Psi_k - \frac{1}{s^2} U_i \right\} - L_c^2 \left\{ \sum_{k=1}^{N+2} E_{ik}^{(4)} \Psi_k - \frac{\nu-1}{r} \sum_{k=1}^{N+2} E_{ik}^{(3)} \Psi_k \right\} \right) \\ - \bar{B} \left(\left\{ \sum_{k=1}^{N+2} E_{ik}^{(2)} \Upsilon_k + \frac{1}{s} \sum_{k=1}^{N+2} E_{ik}^{(1)} \Upsilon_k - \frac{1}{s^2} \Phi_i \right\} - L_c^2 \left\{ \sum_{k=1}^{N+2} E_{ik}^{(4)} \Upsilon_k - \frac{\nu-1}{s} \sum_{k=1}^{N+2} E_{ik}^{(3)} \Upsilon_k \right\} \right) = \{ \bar{I}_1 \Phi_i - \bar{I}_0 U_i \} \Omega_n^2, \\ \bar{C} \left(\sum_{k=1}^{N+2} E_{ik}^{(2)} \Theta_k + \frac{1}{s} \sum_{k=1}^{N+2} E_{ik}^{(1)} \Theta_k - \sum_{k=1}^{N+2} E_{ik}^{(1)} \Upsilon_k - \frac{1}{s} \Phi_i \right) - \bar{C} L_c^2 \left(\sum_{k=1}^{N+2} E_{ik}^{(4)} \Theta_k + \frac{1}{s} \sum_{k=1}^{N+2} E_{ik}^{(3)} \Theta_k - \sum_{k=1}^{N+2} E_{ik}^{(3)} \Upsilon_k - \frac{1}{s} \sum_{k=1}^{N+2} E_{ik}^{(2)} \Upsilon_k \right) = -\bar{I}_0 W_i \Omega_n^2, \end{aligned} \tag{28a}$$



$$\begin{aligned} & \bar{B} \left(\left\{ \sum_{k=1}^{N+2} E_{ik}^{(2)} \Psi_k + \frac{1}{s} \sum_{k=1}^{N+2} E_{ik}^{(1)} \Psi_k - \frac{1}{s^2} U_i \right\} - L_c^2 \left\{ \sum_{k=1}^{N+2} E_{ik}^{(4)} \Psi_k - \frac{\nu-1}{s} \sum_{k=1}^{N+2} E_{ik}^{(3)} \Psi_k \right\} \right) \\ & - \bar{C} \left(\left\{ \sum_{k=1}^{N+2} E_{ik}^{(1)} \Theta_k + \Phi_1 \right\} - L_c^2 \left\{ \sum_{k=1}^{N+2} E_{ik}^{(3)} \Theta_k + \sum_{k=1}^{N+2} E_{ik}^{(2)} \Upsilon_k \right\} \right) - \bar{D} \left(\left\{ \sum_{k=1}^{N+2} E_{ik} \Upsilon_k + \frac{1}{s} \sum_{k=1}^{N+2} E_{ik}^{(1)} \Upsilon_k - \frac{\Phi_1}{s^2} \right\} - L_c^2 \left\{ \sum_{k=1}^{N+2} E_{ik}^{(4)} \Upsilon_k - \frac{\nu-1}{s} \sum_{k=1}^{N+2} E_{ik}^{(3)} \Upsilon_k \right\} \right) = \{ \bar{I}_1 U_i - \bar{I}_2 \Phi_1 \} \Omega_n^2. \end{aligned} \tag{28b}$$

$$\begin{aligned} @s = 1: & \begin{cases} \sum_{k=1}^{N+2} E_{1k}^{(2)} \Psi_k - \frac{1}{L} \sum_{k=1}^{N+2} E_{1k}^{(1)} \Psi_k = 0, & \sum_{k=1}^{N+2} E_{1k}^{(2)} \Upsilon_k - \frac{1}{L} \sum_{k=1}^{N+2} E_{1k}^{(1)} \Upsilon_k = 0 \\ \left(\sum_{k=1}^{N+2} E_{1k}^{(2)} \Theta_k + \sum_{k=1}^{N+2} E_{1k}^{(1)} \Upsilon_k \right) - \frac{1}{L} \left(\sum_{k=1}^{N+2} E_{1k}^{(1)} \Theta_k + \Phi_1 \right) = 0. \end{cases} \\ @s = \alpha: & \begin{cases} \sum_{k=1}^{N+2} E_{Nk}^{(2)} \Psi_k + \frac{1}{L} \sum_{k=1}^{N+2} E_{Nk}^{(1)} \Psi_k = 0, & \sum_{k=1}^{N+2} E_{Nk}^{(2)} \Upsilon_k + \frac{1}{L} \sum_{k=1}^{N+2} E_{Nk}^{(1)} \Upsilon_k = 0, \\ \left(\sum_{k=1}^{N+2} E_{Nk}^{(2)} \Theta_k + \sum_{k=1}^{N+2} E_{Nk}^{(1)} \Upsilon_k \right) + \frac{1}{L} \left(\sum_{k=1}^{N+2} E_{Nk}^{(1)} \Theta_k + \Phi_N \right) = 0. \end{cases} \end{aligned} \tag{29}$$

Also, the boundary conditions for the inner edge can be obtained using Eq. (23) and Table 2 as follows:

$$U_1 = W_1 = \Phi_1 = 0 \tag{30}$$

$$U_1 = W_1 = 0,$$

$$M_{rr} = 0 \Rightarrow \bar{B} \left(\sum_{k=1}^{N+2} E_{1k}^{(1)} \Psi_k + \nu U_1 - L_c^2 \sum_{k=1}^{N+2} E_{1k}^{(3)} \Psi_k \right) + \bar{D} \left(\sum_{k=1}^{N+2} E_{1k}^{(1)} \Upsilon_k + \nu \Phi_1 - L_c^2 \sum_{k=1}^{N+2} E_{1k}^{(3)} \Upsilon_k \right) = 0. \tag{31}$$

$$\{N_{rr}, M_{rr}\} = 0 \Rightarrow \{ \bar{A}, \bar{B} \} \left(\sum_{k=1}^{N+2} E_{1k}^{(1)} \Psi_k + \nu U_1 - L_c^2 \sum_{k=1}^{N+2} E_{1k}^{(3)} \Psi_k \right) + \{ \bar{B}, \bar{D} \} \left(\sum_{k=1}^{N+2} E_{1k}^{(1)} \Upsilon_k + \nu \Phi_1 - L_c^2 \sum_{k=1}^{N+2} E_{1k}^{(3)} \Upsilon_k \right) = 0, \quad W_1 = 0. \tag{32}$$

$$Q_r = 0 \Rightarrow \sum_{k=1}^{N+2} E_{1k}^{(1)} \Theta_k + \Phi_1 - L_c^2 \left(\sum_{k=1}^{N+2} E_{1k}^{(3)} \Theta_k + \sum_{k=1}^{N+2} E_{1k}^{(2)} \Upsilon_k \right) = 0,$$

$$\{N_{rr}, M_{rr}\} = 0 \Rightarrow \{ \bar{A}, \bar{B} \} \left(\sum_{k=1}^{N+2} E_{1k}^{(1)} \Psi_k + \nu U_1 - L_c^2 \sum_{k=1}^{N+2} E_{1k}^{(3)} \Psi_k \right) + \{ \bar{B}, \bar{D} \} \left(\sum_{k=1}^{N+2} E_{1k}^{(1)} \Upsilon_k + \nu \Phi_1 - L_c^2 \sum_{k=1}^{N+2} E_{1k}^{(3)} \Upsilon_k \right) = 0. \tag{33}$$

Finally, the boundary conditions for the outer edge can be written as:

$$U_N = W_N = \Phi_N = 0. \tag{34}$$

$$M_{rr} = 0 \Rightarrow \bar{B} \left(\sum_{k=1}^{N+2} E_{Nk}^{(1)} \Psi_k + \nu \frac{U_N}{\alpha} - L_c^2 \sum_{k=1}^{N+2} E_{Nk}^{(3)} \Psi_k \right) + \bar{D} \left(\sum_{k=1}^{N+2} E_{Nk}^{(1)} \Upsilon_k + \nu \frac{1}{\alpha} \Phi_N - L_c^2 \sum_{k=1}^{N+2} E_{Nk}^{(3)} \Upsilon_k \right) = 0, \quad U_N = W_N = 0. \tag{35}$$

$$\{N_{rr}, M_{rr}\} = 0 \Rightarrow \{ \bar{A}, \bar{B} \} \left(\sum_{k=1}^{N+2} E_{Nk}^{(1)} \Psi_k + \nu \frac{U_N}{\alpha} - L_c^2 \sum_{k=1}^{N+2} E_{Nk}^{(3)} \Psi_k \right) + \{ \bar{B}, \bar{D} \} \left(\sum_{k=1}^{N+2} E_{Nk}^{(1)} \Upsilon_k + \nu \frac{1}{\alpha} \Phi_N - L_c^2 \sum_{k=1}^{N+2} E_{Nk}^{(3)} \Upsilon_k \right) = 0, \quad W_1 = 0. \tag{36}$$

$$\{N_{rr}, M_{rr}\} = 0 \Rightarrow \{ \bar{A}, \bar{B} \} \left(\sum_{k=1}^{N+2} E_{Nk}^{(1)} \Psi_k + \nu \frac{U_N}{\alpha} - L_c^2 \sum_{k=1}^{N+2} E_{Nk}^{(3)} \Psi_k \right) + \{ \bar{B}, \bar{D} \} \left(\sum_{k=1}^{N+2} E_{Nk}^{(1)} \Upsilon_k + \nu \frac{1}{\alpha} \Phi_N - L_c^2 \sum_{k=1}^{N+2} E_{Nk}^{(3)} \Upsilon_k \right) = 0, \tag{37}$$

$$Q_r = 0 \Rightarrow \sum_{k=1}^{N+2} E_{Nk}^{(1)} \Theta_k + \Phi_N - L_c^2 \left(\sum_{k=1}^{N+2} E_{Nk}^{(3)} \Theta_k + \sum_{k=1}^{N+2} E_{Nk}^{(2)} \Upsilon_k \right) = 0.$$

In a similar form as shown in Refs. [80, 81], the assembled form can be presented such as Eq. (38) by rearranging Eq. (28) to Eq. (37):

$$\begin{bmatrix} [S_{bb}] & [S_{bd}] \\ [S_{db}] & [S_{dd}] \end{bmatrix} \begin{Bmatrix} \{U_b\} \\ \{U_d\} \end{Bmatrix} - \Omega_n^2 \begin{bmatrix} [0] & [0] \\ [Q_{db}] & [Q_{dd}] \end{bmatrix} \begin{Bmatrix} \{U_b\} \\ \{U_d\} \end{Bmatrix} = \begin{Bmatrix} \{0\} \\ \{0\} \end{Bmatrix} \tag{38}$$

where,

$$\begin{aligned} \{q_b\} &= \{q_1, \dots, q_6, q_{3N+1}, \dots, q_{3N+6}\} = \{U_1^{(1)}, W_1^{(1)}, \Phi_1^{(1)}, U_1, W_1, \Phi_1, U_N, W_N, \Phi_N, U_N^{(1)}, W_N^{(1)}, \Phi_N^{(1)}\}, \\ \{U_d\} &= \{U_6, U_7, \dots, U_{2N}, U_{2N+1}\} = \{U_2, W_2, \Phi_2, \dots, U_{N-1}, W_{N-1}, \Phi_{N-1}\}. \end{aligned} \tag{39}$$

Applying the matrix sub-structuring method, Eq. (38) can be written into the following generalized eigenvalue equation:

$$([S] - \Omega_n^2 [Q]) \{U_d\} = \{0\} \tag{40}$$

where,

$$[S] = [S_{dd}] - [S_{db}] [S_{bb}]^{-1} [S_{bd}], \quad [Q] = [Q_{dd}] - [Q_{db}] [S_{bb}]^{-1} [S_{bd}] \tag{41}$$

The non-dimensional frequencies of the annular nano-plate, Ω_n , can be obtained by solving the Eq. (40).



Table 3. Mechanical properties of FGM annular nano-plate.

$k=\pi^2/12$	$\nu = 0.3$	$\rho_m = 7860 \text{ (Kg/m}^3\text{)}$	$\rho_c = 3600 \text{ (Kg/m}^3\text{)}$	$E_m = 211 \text{ (Gpa)}$	$E_c = 380 \text{ (Gpa)}$
--------------	-------------	---	---	---------------------------	---------------------------

Table 4. Comparison of solution in Ref. [82] (GDQ with N=16) and numerical method for first dimensionless natural frequency of the annular plate ($L_c = 0, n = 0, N = 10$). The inside B.C. is clamped.

Outside B.C.s	h/b	Solution method	$\Omega_1 = \omega_1 b^2 \sqrt{\rho h/D}$		
			a/b = 0.1	a/b = 0.2	a/b = 0.3
Clamped	0.05	Ref. [82],	26.534	33.533	43.599
		GDQR (Present work)	26.535	33.534	43.600
	0.1	Ref. [82],	24.629	30.841	39.398
		GDQR (Present work)	24.628	30.841	39.398
Simply support	0.05	Ref. [82],	17.460	22.262	29.256
		GDQR (Present work)	17.461	22.262	29.255
	0.1	Ref. [82],	16.575	21.057	27.379
		GDQR (Present work)	16.575	21.057	27.379
Free	0.05	Ref. [82],	4.215	5.155	6.623
		GDQR (Present work)	4.216	5.154	6.623
	0.1	Ref. [82],	4.150	5.079	6.516
		GDQR (Present work)	4.151	5.080	6.516

Table 5. Comparison of solution in Ref. [82] (GDQ with N=16) and numerical method for first dimensionless natural frequency of the annular plate ($L_c = 0, n = 0, N = 10$). The inside B.C. is simply supported.

Outside B.C.s	h/b	Solution method	$\Omega_1 = \omega_1 b^2 \sqrt{\rho h/D}$		
			a/b = 0.1	a/b = 0.2	a/b = 0.3
Clamped	0.05	Ref. [82],	22.294	26.242	33.003
		GDQR (Present work)	22.294	26.241	33.002
	0.1	Ref. [82],	21.200	24.916	31.010
		GDQR (Present work)	21.199	24.916	31.102
Simply support	0.05	Ref. [82],	14.324	16.618	20.852
		GDQR (Present work)	14.324	16.618	20.852
	0.1	Ref. [82],	13.874	16.164	20.219
		GDQR (Present work)	13.874	16.163	20.218
Free	0.05	Ref. [82],	3.437	3.332	3.416
		GDQR (Present work)	3.437	3.331	3.416
	0.1	Ref. [82],	3.400	3.309	3.398
		GDQR (Present work)	3.400	3.309	3.397

6. Validation of the Solution Method

A comparison has been made with other articles to check the correctness of the results. Also, the convergence of the obtained frequencies for the two models of stress-driven method and strain gradient theory has been investigated for different values of the size parameter in different boundary conditions. The mechanical properties of the FGM annular nano-plate are shown in Table 3.

Reference [82] investigates the vibrations of annular plates made of isotropic homogeneous materials. In this reference, the effects of the ratio of inner diameter to the outer diameter and the boundary conditions on the natural frequency have been investigated by GDQ solution using local first-order shear deformation. To evaluate the efficiency of the solution method proposed in this paper, GDQR, the value of the first symmetric natural frequency for various boundary conditions is calculated and compared with the reference results mentioned in Tables 4-5. In order to achieve the results based on the local FSDT for isotropic homogeneous material, the size parameter, L_c , and the composite heterogeneity index n have been considered equal to zero. As can be seen, the results of the method presented in this article have good accuracy.

Also, the convergence rate of the first symmetric dimensionless frequency of FGM annular plate is evaluated for different values of the size parameter, aspect ratio $h/b=0.1$, $a/b=0.2$ and the inhomogeneity index $n=1$ and any boundary conditions for the inner and outer edge of the annular plate. The results are shown in Figs. 6-9 as the magnitude of N is increased. As observed, The GDQR method is well applicable to the vibrational analysis of the FGM annular plate, with a fast convergence rate as N approaches 10.

7. Result and Discussion

According to the equations of motion derived based on the nonlocal SDM and FSDT, there are a few parameters that influence the vibrational behavior of the FGM annular nano-plate. These factors can be grouped as the material and geometry related factors; namely the size parameter L_c , heterogeneity index n , aspect ratios h/b , a/b , and the boundary conditions as shown in Figs. 2-5.

To investigate the effect of size parameter L_c , the ratio of the fundamental (first axisymmetric) natural frequency of the presented structure based on the nonlocal SDM and FSDT to the fundamental natural frequency of that based on local FSDT, $\Omega_{SDM,FSDT} / \Omega_{local,FSDT}$, versus the size parameter L_c is generated based on different types of conditions for four cases with $h/b = \{0.05, 0.1\}$ and $a/b = \{0.2, 0.3\}$. These results are shown in Fig. 10-13. Additionally, to investigate the effect of aspect ratios a/b and h/b , the ratio of the fundamental natural frequency of the presented structure based on the nonlocal SDM and FSDT to the fundamental natural frequency of that based on the SDM and CLPT, $\Omega_{SDM,FSDT} / \Omega_{SDM,CLPT}$, versus the aspect ratios a/b and h/b are plotted for different types of conditions as shown in Figs. 14 to 21. Finally, to assess the effect of heterogeneity index n on the vibrational behavior of the FGM annular nano-plate, the fundamental frequency of the presented structure based on the nonlocal SDM and FSDT is calculated for the cases with aspect ratios $a/b = h/b = 0.1$ and $L_c = \{0.00, 0.05, 0.10\}$. Also, these results are shown in Figs. 22 to 25. These results are based on the values of 0.3 and 20 selected for the Poisson's ratio and the number of divisions for the presented numerical solution (GDQR), respectively, and the other mechanical properties of the FGM annular nano-plate are given in Table 3.



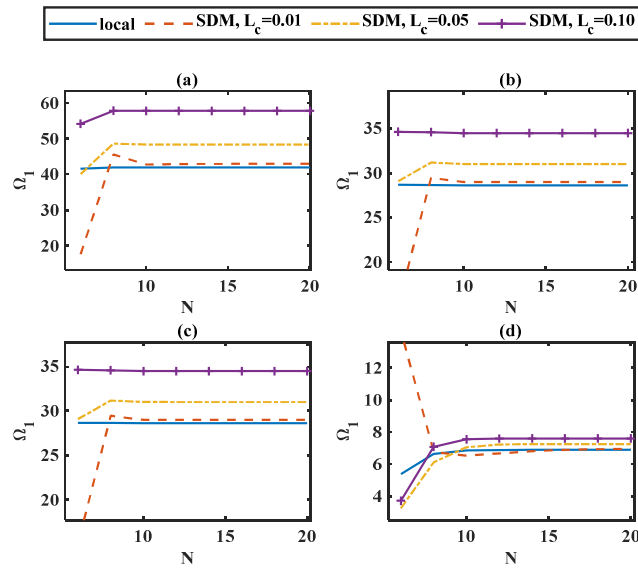


Fig. 6. Evaluating the convergence rate of the first symmetric dimensionless frequency of FGM annular plate, based on the different size parameters and (a) C-C, (b) C-KS, (c) C-SS, and (d) C-F boundary conditions with $n=1$, $h/b=0.1$ and $a/b=0.2$.

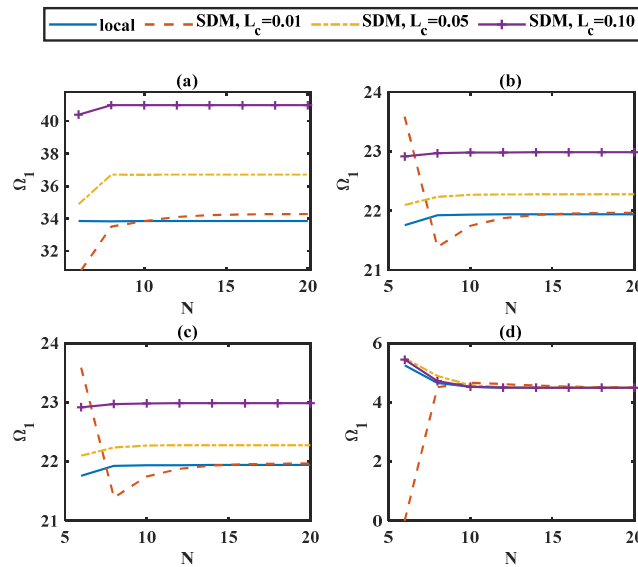


Fig. 7. Evaluating the convergence rate of the first symmetric dimensionless frequency of FGM annular plate, based on the different size parameters and (a) KS-C, (b) KS-KS, (c) KS-SS, and (d) KS-F boundary conditions with $n=1$, $h/b=0.1$ and $a/b=0.2$.

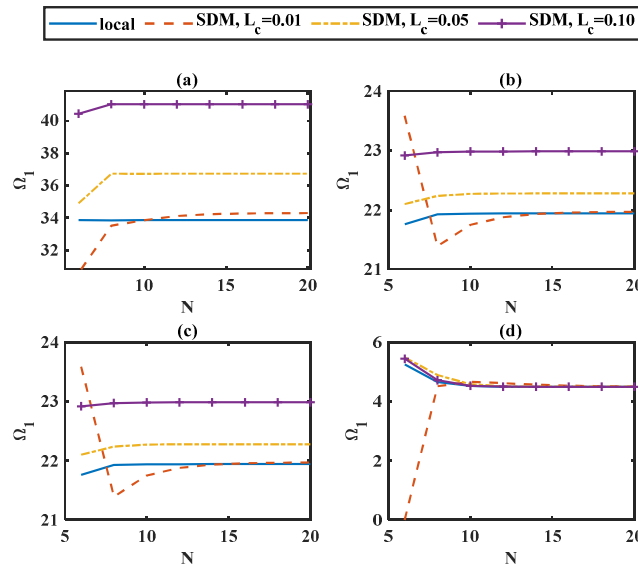


Fig. 8. Evaluating the convergence rate of the first symmetric dimensionless frequency of FGM annular plate, based on the different size parameters and (a) C-C, (b) C-KS, (c) C-SS, and (d) C-F boundary conditions with $n=1$, $h/b=0.1$ and $a/b=0.2$.



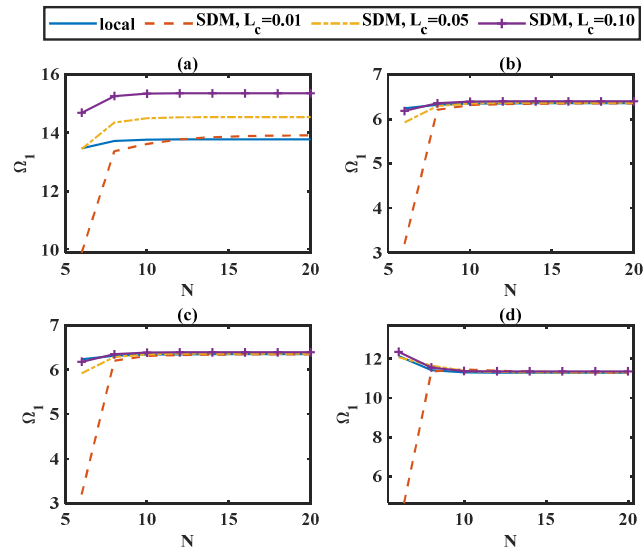


Fig. 9. Evaluating the convergence rate of the first symmetric dimensionless frequency of FGM annular plate, based on the different size parameters and (a) KS-C, (b) KS-KS, (c) KS-SS, and (d) KS-F boundary conditions with $n=1$, $h/b=0.1$ and $a/b=0.2$

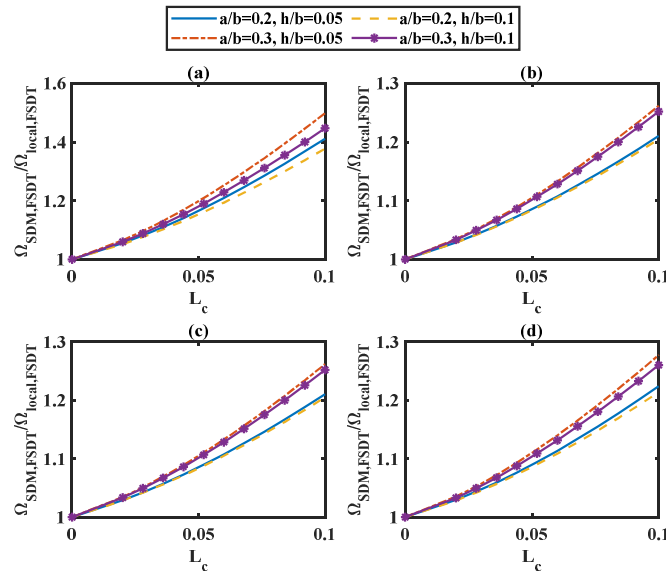


Fig. 10. The effect of size parameter L_c on the frequency ratio of the annular FGM, $\Omega_{SDM,FSDT} / \Omega_{local,FSDT}$, with (a) C-C, (b) C-KS, (c) C-SS, and (d) C-F conditions with $n=1$.

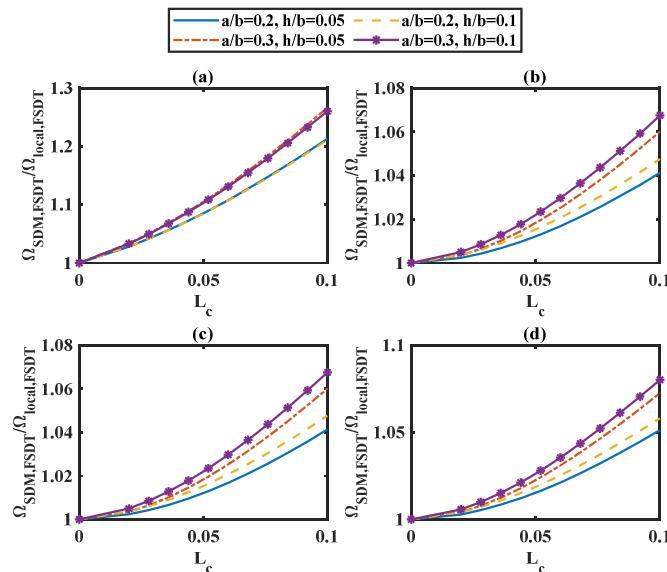


Fig. 11. The effect of size parameter L_c on the frequency ratio of the annular FGM, $\Omega_{SDM,FSDT} / \Omega_{local,FSDT}$, with (a) KS-C, (b) KS-KS, (c) KS-SS, and (d) KS-F conditions with $n=1$.



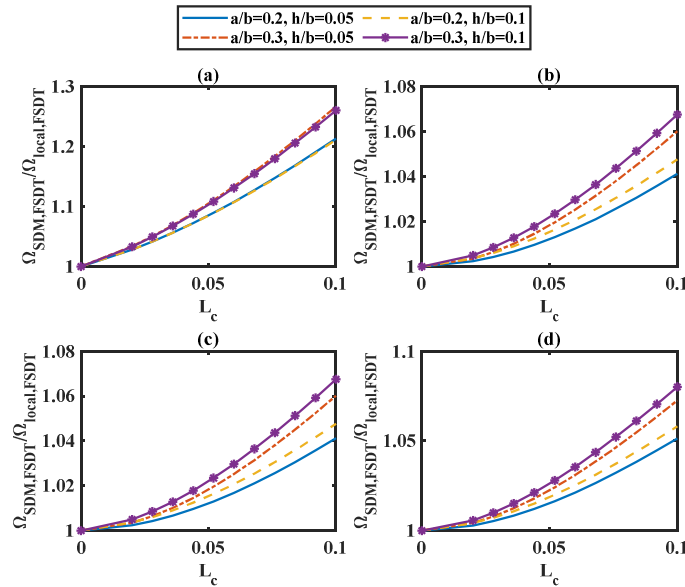


Fig. 12. The effect of size parameter L_c on the frequency ratio of the annular FGM, $\Omega_{SDM,FSDT}/\Omega_{local,FSDT}$, with a (a) SS-C, (b) SS-KS, (c) SS-SS, and (d) SS-F conditions with $n=1$.

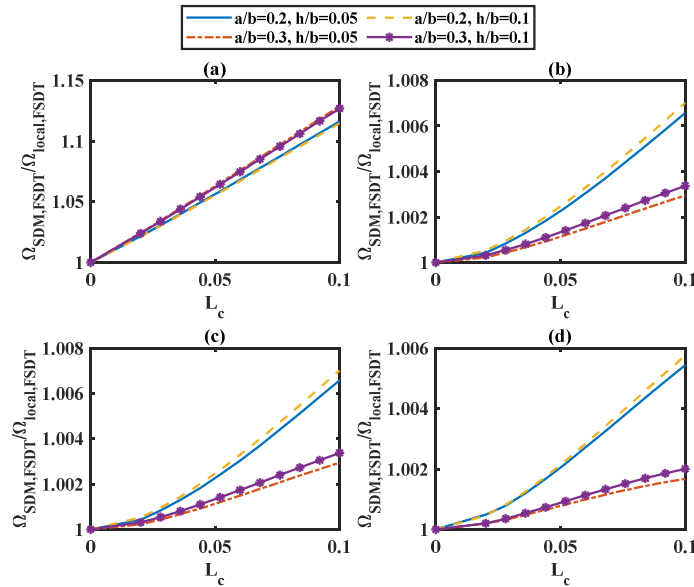


Fig. 13. The effect of size parameter L_c on the frequency ratio of the annular FGM, $\Omega_{SDM,FSDT}/\Omega_{local,FSDT}$, a (a) F-C, (b) F-KS, (c) F-SS, and (d) F-F conditions with $n=1$.

7.1 Size parameter, L_c , effect on the vibrational behavior

Firstly, the fundamental natural frequency of FGM annular nano-plate for different cases with aspect ratios $h/b = \{0.2, 0.3\}$ and $a/b = \{0.2, 0.3\}$ with different types of boundary conditions for two models, local and nonlocal SDM based on FSDT, are extracted. Then the frequency ratio, $\Omega_{SDM,FSDT}/\Omega_{local,FSDT}$ is determined and plotted versus the size parameter L_c in Figs. 10-13.

According to Figs. 10-13, the vibrational frequency is well dependent on the size parameter as well as the type of boundary condition imposed on the plate edges. As can be seen, with the increase in size parameter L_c , the frequency ratio increases for all types of boundary conditions and aspect ratios. This indicates that the use of nonlocal SDM and FSDT leads to stiffening of the structure and thus the value of natural frequency increases compared to the local FSDT model. This phenomenon is very similar to the strain gradient theory [31-37] that has been proven physically (statistically) based on the theories for rubber-like materials by deriving a physically based strain gradient continuum by Jiang et al. [35].

Furthermore, these results show that for modeling structures in nanoscale with any boundary conditions, non-local models must be used instead of the local model. It is also observed that the amount of increase of the frequency ratio is different for different values of the aspect ratios a/b and h/b , which will be investigated in terms of their effect on the vibrational behavior of the structure.

7.2 Aspect ratio, a/b , effect on the vibrational behavior

The fundamental natural frequency of FGM annular nano-plate for different types of boundary conditions, size parameters, $L_c = \{0.00, 0.05, 0.10\}$ and aspect ratio $h/b=0.1$ is extracted based on the SDM together with the CLPT and FSDT. Then the frequency ratio, $\Omega_{SDM,FSDT}/\Omega_{SDM,CLPT}$, is determined and plotted versus the aspect ratios a/b in Figs. 14-17. In this case, the result for $L_c=0.00$ is nominated “local”.



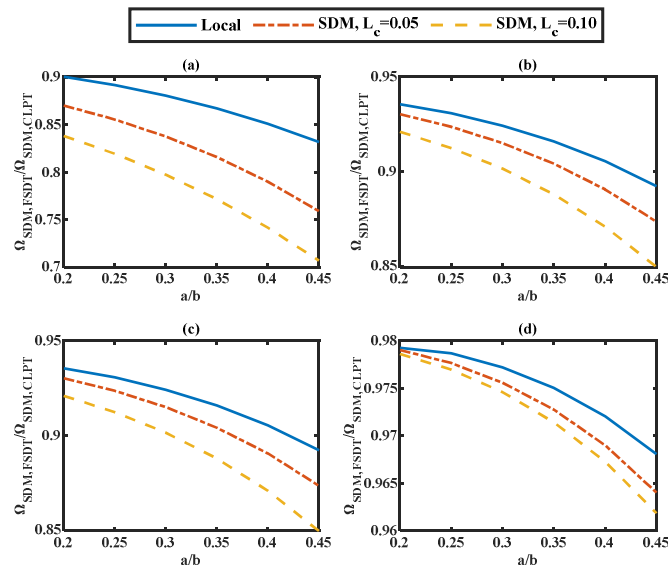


Fig. 14. The effect of aspect ratio a/b on the frequency ratio of the annular FGM, R_2 , with (a) C-C, (b) C-KS, (c) C-SS, and (d) C-F conditions with $h/b=0.1$, and $n=1$.

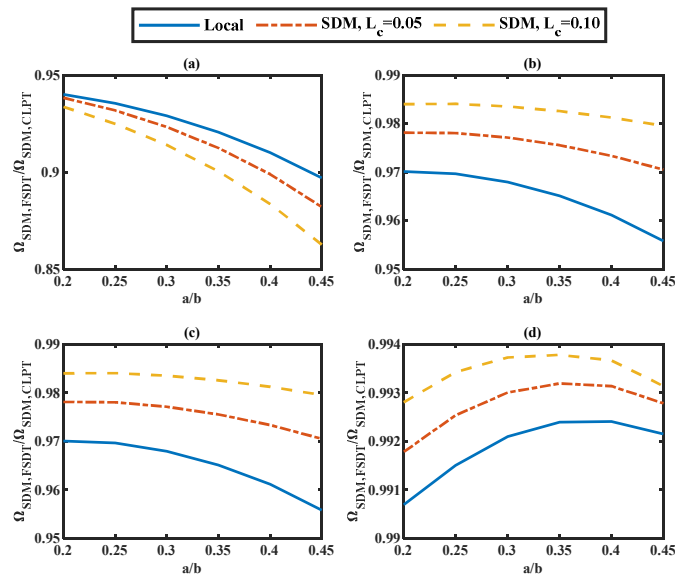


Fig. 15. The effect of aspect ratio a/b on the frequency ratio of the annular FGM, R_2 , with (a) KS-C, (b) KS-KS, (c) KS-SS, and (d) KS-F conditions and $h/b=0.1$, and $n=1$.

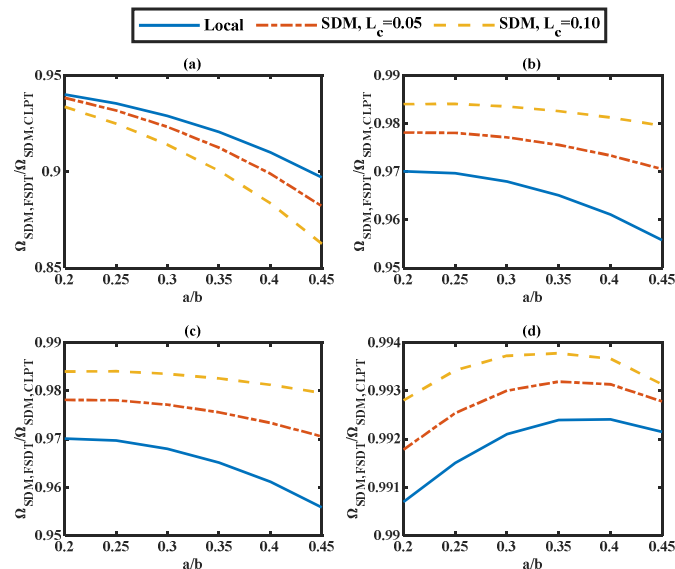


Fig. 16. The effect of aspect ratio a/b on the frequency ratio of the annular FGM, R_2 , with (a) SS-C, (b) SS-KS, (c) SS-SS, and (d) SS-F conditions with $h/b=0.1$ and $n=1$.



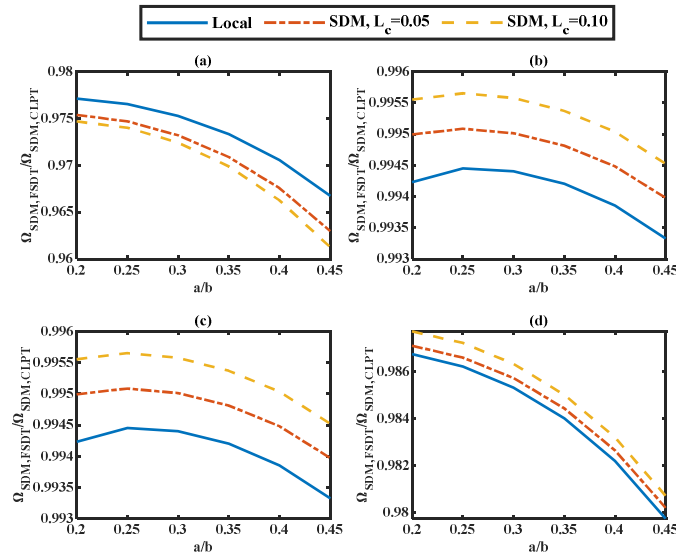


Fig. 17. The effect of aspect ratio a/b on the frequency ratio of the annular FGM, R_2 , with (a) F-C, (b) F-KS, (c) F-SS, and (d) F-F conditions with $h/b=0.1$, and $n=1$.

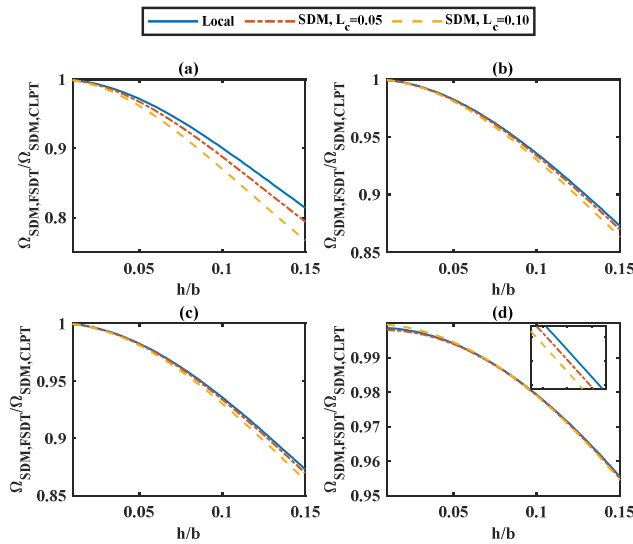


Fig. 18. The effect of aspect ratio h/b on the frequency ratio of the annular FGM, $\Omega_{SDM,FSDT}/\Omega_{SDM,CLPT}$, with (a) C-C, (b) C-KS, (c) C-SS, and (d) C-F conditions with $a/b=0.2$ and $n=1$.

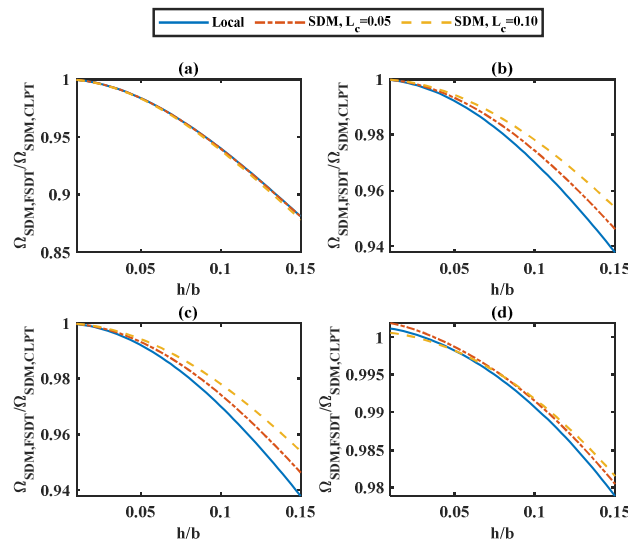


Fig. 19. The effect of aspect ratio h/b on the frequency ratio of the annular FGM, $\Omega_{SDM,FSDT}/\Omega_{SDM,CLPT}$, with (a) KS-C, (b) KS-KS, (c) KS-SS, and (d) KS- conditions with $a/b=0.2$ and $n=1$.



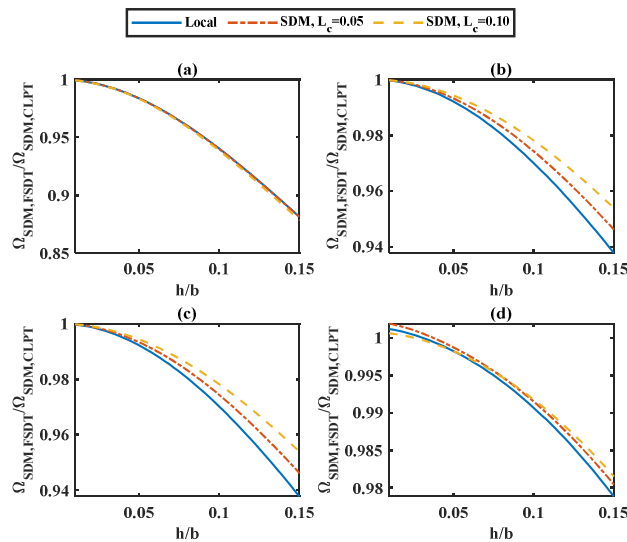


Fig. 20. The effect of aspect ratio h/b on the frequency ratio of the annular FGM, $\Omega_{SDM,FSDT} / \Omega_{SDM,CLPT}$, with (a) SS-C, (b) SS-KS, (c) SS-SS, and (d) SS-F conditions with $a/b=0.2$ and $n=1$.

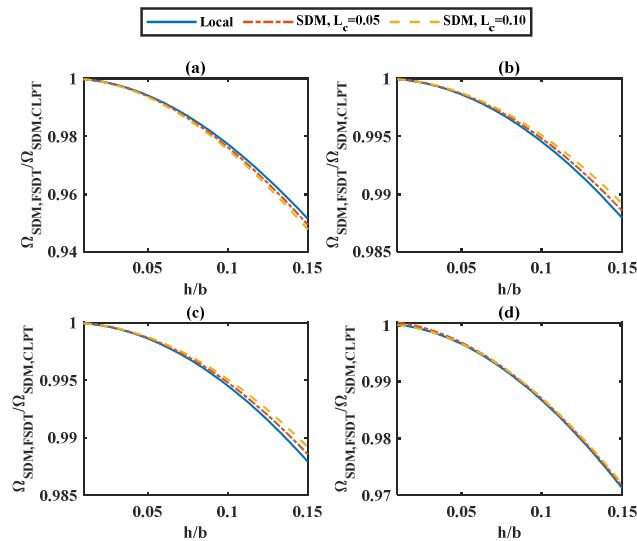


Fig. 21. The effect of aspect ratio h/b on the frequency ratio of the annular FGM, $\Omega_{SDM,FSDT} / \Omega_{SDM,CLPT}$, with (a) F-C, (b) F-KS, (c) F-SS, and (d) F-F conditions with $a/b=0.2$ and $n=1$.

According to these figures, the vibrational frequency is well dependent on the aspect ratio a/b as well as the type of boundary condition imposed on the plate edges. It can be shown that in Figs. 14, 15(a), 16(a), and 17(a) for the plate with C-C, C-KS, C-SS, C-F, KS-C, SS-C and F-C boundary conditions, with an increase in aspect ratio a/b , the aforementioned frequency ratio decreases. The highest and lowest value for this ratio belongs to the local and nonlocal model with the size parameter $L_c=0.10$. On the other hand, by increasing aspect ratio a/b , the difference between the results of the local and nonlocal model increases and indicate that using nonlocal SDM and FSDT is more vital to model the presented structure for the higher value of size parameter L_c and aspect ratio a/b .

Based on Figs. 15(b, c), 16(b, c) and 17(d) for the plate with KS-KS, KS-SS, SS-KS, SS-SS and F-F boundary conditions, with the increase in aspect ratio a/b , the frequency ratio decreases. The lowest and highest value for frequency ratio belongs to the local and nonlocal model with the size parameter $L_c=0.10$. Except for the F-F boundary condition, by increasing aspect ratio a/b , the difference between the results of the local and nonlocal model increases and indicate that the use of nonlocal SDM and FSDT is more vital to model the presented structure for a lower value of size parameter L_c and higher value of aspect ratio a/b for mentioned boundary conditions except for the F-F boundary condition. Additionally, for the F-F boundary condition use of nonlocal SDM and FSDT is more vital to model the presented structure for a lower value of size parameter L_c and aspect ratio a/b .

According to Figs. 15(d), 16(d) for the plate with KS-F and SS-F boundary conditions, with the increase in aspect ratio a/b for values up to nearly 0.35, the frequency ratio increases and decreases beyond that. Also, for these boundary conditions, the highest and lowest value for frequency ratio belongs to the local and nonlocal model with the size parameter $L_c=0.10$. Although, by increasing aspect ratio a/b , the difference between the results of the local and nonlocal model decreases. These results indicate that the use of nonlocal SDM and FSDT is more vital to model the presented structure for a lower value of size parameter L_c when the aspect ratio a/b increases and decreases from value 0.35.

According to Figure 17(b, c) for the plate with F-KS and F-SS boundary conditions, with the increase in aspect ratio a/b for values up to nearly 0.25, the frequency ratio increases and decreases beyond that. Also, for these boundary conditions, the highest and lowest value for frequency ratio belongs to the local and nonlocal model with the size parameter $L_c=0.10$. Although, by increasing aspect ratio a/b , the difference between the results of the local and nonlocal model decreases. These results indicate that the use of nonlocal SDM and FSDT is more vital to model the presented structure for a higher value of size parameter L_c when the aspect ratio a/b increases and decreases from value 0.25.



7.3 Aspect ratio, h/b , effect on the vibrational behavior

Like the previous section, the frequency ratio, $\Omega_{SDM,FSDT} / \Omega_{SDM,CLPT}$, is determined and plotted versus the aspect ratios h/b in Figs. 18-21 for different types of boundary conditions and size parameters, $L_c = \{0.00, 0.05, 0.1\}$ and aspect ratio $a/b = 0.2$. In this case, the result for $L_c = 0.00$ is nominated "local" in Figs. 18-21. According to these figures, the vibrational frequency is well dependent on the aspect ratio h/b as well as the type of boundary condition imposed on the plate edges and with the increase in aspect ratio h/b , the frequency ratio decreases.

According to Figs. 18, 19(a), 20(a) and 21 (a) for the plate with C-C, C-KS, C-SS, C-F, KS-C, SS-C and F-C boundary conditions, the highest and lowest value for frequency ratio belong to the local and nonlocal model with the size parameter $L_c = 0.10$. Although, by increasing the aspect ratio h/b , the difference between the results of the local and nonlocal model increases. Except for the C-C boundary condition, this increase is less prominent for another mentioned boundary condition. In fact, this increase is more prominent for C-C boundary condition with larger aspect ratio h/b and size parameter L_c . These results indicate that the use of nonlocal SDM and FSĐT is more vital to model the presented structure C-C boundary condition, for a higher value of size parameter L_c and aspect ratio h/b .

Additionally, based on Figs. 19(b, c, d), 20(b, c, d) and 21(b, c, d), for the plate with KS-KS, KS-SS, KS-F, SS-KS, SS-SS, SS-F, F-KS, F-SS and F-boundary conditions, the lowest and highest value for frequency ratio belong to the local and nonlocal model with the size parameter $L_c = 0.10$. Although, by increasing the aspect ratio h/b , the difference between the results of the local and nonlocal model increases. Except for the F-F boundary condition, this increase is more prominent for another mentioned boundary condition with a larger aspect ratio h/b and size parameter and using nonlocal SDM and FSĐT is more vital to model the presented structure with mentioned boundary condition, for a higher value of size parameter L_c and aspect ratio h/b .

7.4 Heterogeneity index, n , effect on the vibrational behavior

To analyze the effect of heterogeneity index n on the vibrational behavior of the annular FGM nano-plate, the fundamental natural frequency of the presented structure is extracted for different types of boundary conditions, size parameters, $L_c = \{0.00, 0.05, 0.1\}$ and aspect ratios $a/b = h/b = 0.1$ based on SDM and FSĐT. These results are shown in Figs. 22-25. In this case, the result for $L_c = 0.0$ is nominated "local".

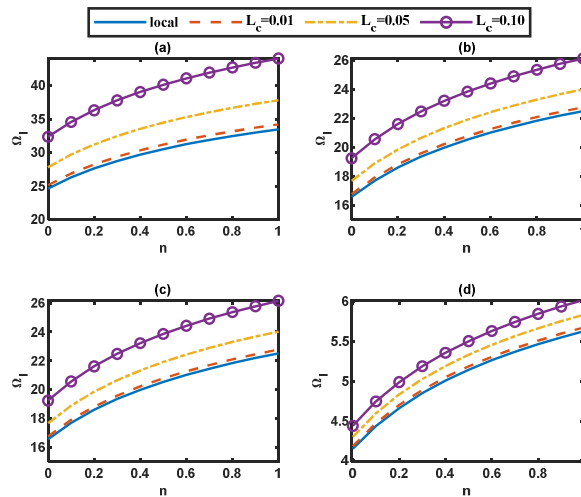


Fig. 22. Influence of material inhomogeneity parameter n and boundary conditions on the first natural frequency of annular FGM nano-plate with (a) C-C, (b) C-KS, (c) C-SS, and (d) C-F conditions and $a/b = h/b = 0.1$.

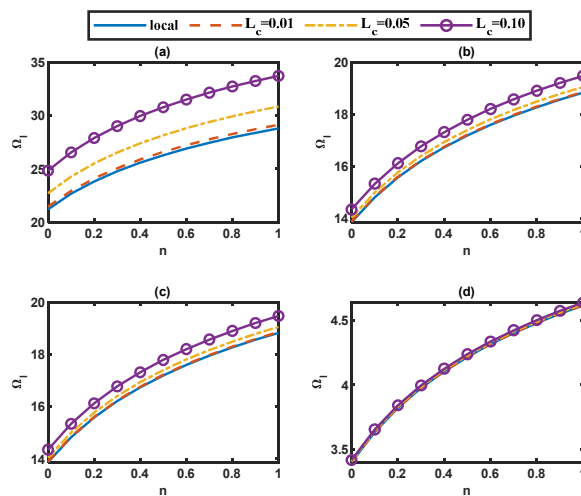


Fig. 23. Influence of material inhomogeneity parameter n and boundary conditions on the first natural frequency of annular FGM nano-plate with (a) KS-C, (b) KS-KS, (c) KS-SS, and (d) KS-F conditions and $a/b = h/b = 0.1$.



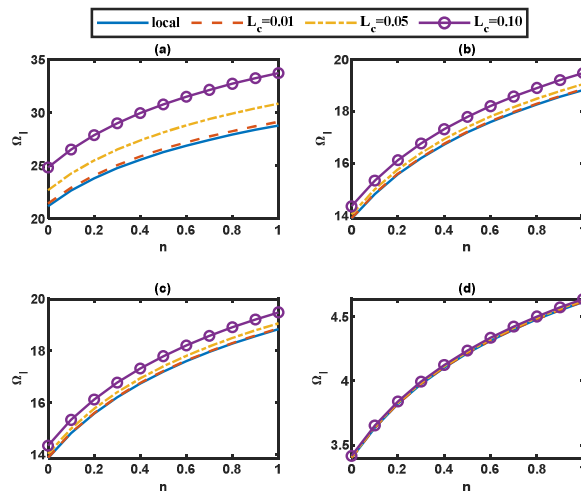


Fig. 24. Influence of material inhomogeneity parameter n and boundary conditions on the first natural frequency of annular FGM nano-plate with (a) SS-C, (b) SS-KS, (c) SS-SS, and (d) SS-F conditions and $a/b = h/b = 0.1$.

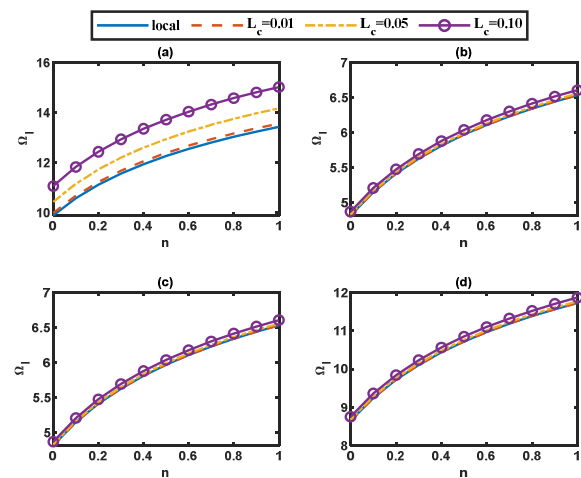


Fig. 25. Influence of material inhomogeneity parameter n and boundary conditions on the first natural frequency of annular FGM nano-plate with (a) F-C, (b) F-KS, (c) F-SS, and (d) F-F conditions and $a/b = h/b = 0.1$.

According to these figures, increasing the material index, n , increases the value of natural frequency for all types of boundary conditions imposed on the plate edges. Also, with the increase in size parameter L_c , the difference between the results of the local and nonlocal model increase. This increase is more prominent for C-C, C-KS, C-SS, C-F, KS-C, SS-C and F-C boundary conditions and less prominent for other boundary conditions. These results indicate that the use of nonlocal SDM is more vital to model the presented structure with C-C, C-KS, C-SS, C-F, KS-C, SS-C and F-C boundary conditions for all values of size parameter L_c and aspect ratio h/b .

8. Conclusion

The non-local stress-driven method was utilized to analyze and investigate the vibration of functionally graded annular nano-plate. The equation of motion and related boundary conditions were solved by the generalized differential quadrature rule. The natural frequency of nano-plate was calculated for different boundary conditions, different inner and outer radiuses, different inhomogeneity parameters, different thicknesses, and different size parameters. The results are compared with those found in other articles. The accuracy of the numerical method used to solve this problem is very good. This method has also rapid (fast) convergence in solving this problem. The non-local stress-driven model predicts the same behavior for different values of a parameter while the strain-driven model predicts different behaviors. For example, the strain-driven method predicts stiffer behavior for some values of size parameter values and softer behavior for others, while the stress-driven method predicts the same behavior for all values of size parameter. According to the results obtained in this research, the use of stress-driven method along with generalized differential quadrature rule is suggested to engineers to solve similar problems.

Author Contributions

M. Shariati planned the scheme, initiated the project and developed the mathematical modeling and solution procedure; M. Shishehsaz and R. Mosalmani examined the theory validation and discussed the results, reviewed, and approved the final version of the manuscript.

Acknowledgments

Not applicable.



Conflict of Interest

The authors declared no potential conflicts of interest concerning the research, authorship, and publication of this article.

Funding

The authors received no financial support for the research, authorship, and publication of this article.

Data Availability Statements

The datasets generated and/or analyzed during the current study are available from the corresponding author on reasonable request.

Nomenclature

E	Elastic modulus [GPa]	$\varepsilon_{rr}^0, \varepsilon_{\theta\theta}^0$	The normal radial and hoop local elastic strains associated with the mid-plane surface
ρ	Density [Kg/m^3]	ϕ	Angular rotation of the normal to the middle surface in radial direction
ν	Poisson's ratio	$\kappa_{rr}, \kappa_{\theta\theta}$	The curvature of the nano-plate along r and θ axes
n	Heterogeneity index of the FG material	$N_{rr}, N_{\theta\theta}, Q_r, M_{rr}, M_{\theta\theta}$	Stress resultants
m	Indices specify the metallic phases of FG material	$\sigma_{rr}, \sigma_{\theta\theta}, \tau_{rz}$	Stress components
c	Indices specify the ceramic phases of FG material	I_0, I_1, I_2	Inertial constants
V	Volume ratio	L, L_c	The dimensional and non-dimensional material size parameter
u_r, u_z	Radial and transverse components of the displacement field	φ_L	Kernel function
u_0, w_0	Displacement functions along the radial and transverse axes of the nano-plate mid-plane	ω_n, Ω_n	Natural frequency and dimensionless natural frequency
A, B, D	Elastic constants of the circular nano-plate	$L(x)$	Legendre interpolation function
$\varepsilon_{rr}, \varepsilon_{\theta\theta}, \gamma_{rz}$	Strain components		

References

- [1] Saeedi, M., et al., Applications of nanotechnology in drug delivery to the central nervous system, *Biomedicine & Pharmacotherapy*, 111, 2019, 666-675.
- [2] Farokhzad, O.C., Nanotechnology for drug delivery: the perfect partnership, *Expert Opinion on Drug Delivery*, 5(9), 2008, 927-929.
- [3] McDonald, T.O., et al., *The application of nanotechnology to drug delivery in medicine*, in Nanoengineering, Elsevier, 2015.
- [4] Mamalis, A., Recent advances in nanotechnology, *Journal of Materials Processing Technology*, 181(1-3), 2007, 52-58.
- [5] Singh, A., Dubey, S., Dubey, H.K., Nanotechnology: The future engineering, *Nanotechnology*, 6(2), 2019, 230-3.
- [6] Geer, D., Nanotechnology: the growing impact of shrinking computers, *IEEE Pervasive Computing*, 5(1), 2006, 7-11.
- [7] Khan, S., et al., Engineered nanoparticles for removal of pollutants from wastewater: Current status and future prospects of nanotechnology for remediation strategies, *Journal of Environmental Chemical Engineering*, 9(5), 2021, 106160.
- [8] Mehndiratta, P., et al., Environmental pollution and nanotechnology, *Environment and Pollution*, 2(2), 2013, 49.
- [9] Abu-Lebdeh, Y., Davidson, I., *Nanotechnology for lithium-ion batteries*, Springer Science & Business Media, 2012.
- [10] Suryatna, A., et al., A review of high-energy density lithium-air battery technology: Investigating the effect of oxides and nanocatalysts, *Journal of Chemistry*, 2022, 2022, 2762647.
- [11] Ambaye, A.D., et al., Recent developments in nanotechnology-based printing electrode systems for electrochemical sensors, *Talanta*, 225, 2021, 121951.
- [12] Kumar, H., et al., Applications of nanotechnology in sensor-based detection of foodborne pathogens, *Sensors*, 20(7), 2020, 1966.
- [13] Yarlagaadda, T., et al., Recent developments in the Field of nanotechnology for development of medical implants, *Procedia Manufacturing*, 30, 2019, 544-551.
- [14] Calisir, M., *Nanotechnology in dentistry: past, present, and future*, in Nanomaterials for Regenerative Medicine, Springer, 2019.
- [15] Singh, V.K., et al., *Nanotechnology and Manufacturing*, in Advanced Manufacturing Processes, CRC Press, 2022.
- [16] Sinha, A., Behera, A., *Nanotechnology in the space industry*, in Nanotechnology-Based Smart Remote Sensing Networks for Disaster Prevention, Elsevier, 2022.
- [17] Skoczylas, J., Samborski, S., Kłonica, M., The application of composite materials in the aerospace industry, *Journal of Technology and Exploitation in Mechanical Engineering*, 5(1), 2019, doi: 10.35784/jteme.73.
- [18] Viscardi, M., et al., Multi-functional nanotechnology integration for aeronautical structures performance enhancement, *International Journal of Structural Integrity*, 9(6), 2018, 737-752.
- [19] Gobato, R., et al., New Nano-Molecule Kurumi-C13H 20BeLi2SeSi/C13H19BeLi2SeSi, and Raman Spectroscopy Using ab initio, Hartree-Fock Method in the Base Set CC-pVTZ and 6-311G**(3df, 3pd), *Journal of Analytical & Pharmaceutical Research*, 8(1), 2019, 1-6.
- [20] Zhang, L., et al., Laboratory evaluation of rheological properties of asphalt binder modified by nano-tio2/caco3, *Advances in Materials Science and Engineering*, 2021, 2021, 5522025.
- [21] Zhou, F., et al., Experimental study on nano silica modified cement base grouting reinforcement materials, *Geomechanics and Engineering*, 20(1), 2020, 67-73.
- [22] Azizi, B., et al., A comprehensive study on the mechanical properties and failure mechanisms of graphyne nanotubes (GNTs) in different phases, *Computational Materials Science*, 182, 2020, 109794.
- [23] Ghafouri Pourkermani, A., Azizi, B., Nejat Pishkenari, H., Vibrational analysis of Ag, Cu and Ni nanobeams using a hybrid continuum-atomistic model, *International Journal of Mechanical Sciences*, 165, 2020, 105208.
- [24] Momen, R., et al., Evaluation of mechanical properties of multilayer graphyne-based structures as anode materials for lithium-ions batteries, *The*



European Physical Journal Plus, 137(3), 2022, 360.

- [25] Shariati, M., Souq, S.S.M.N., Azizi, B., Surface- and nonlocality-dependent vibrational behavior of graphene using atomistic-modal analysis, *International Journal of Mechanical Sciences*, 228, 2022, 107471.
- [26] Eringen, A.C., Edelen, D.G.B., On nonlocal elasticity, *International Journal of Engineering Science*, 10(3), 1972, 233-248.
- [27] Pradhan, S., Phadikar, J., Nonlocal elasticity theory for vibration of nanoplates, *Journal of Sound and Vibration*, 325(1-2), 2009, 206-223.
- [28] Liew, K., Zhang, Y., Zhang, L., Nonlocal elasticity theory for graphene modeling and simulation: prospects and challenges, *Journal of Modeling in Mechanics and Materials*, 1(1), 2017, 20160159.
- [29] Lim, C., Zhang, G., Reddy, J.N., A higher-order nonlocal elasticity and strain gradient theory and its applications in wave propagation, *Journal of the Mechanics and Physics of Solids*, 78, 2015, 298-313.
- [30] Aksencer, T., Aydogdu, M., Levy type solution method for vibration and buckling of nanoplates using nonlocal elasticity theory, *Physica E: Low-dimensional Systems and Nanostructures*, 43(4), 2011, 954-959.
- [31] Adeli, M.M., et al., Torsional vibration of nano-cone based on nonlocal strain gradient elasticity theory, *The European Physical Journal Plus*, 132(9), 2017, 393.
- [32] De Domenico, D., Askes, H., Aifantis, E.C., Discussion of "Derivation of Mindlin's first and second strain gradient elastic theory via simple lattice and continuum models" by Polyzos and Fotiadis, *International Journal of Solids and Structures*, 191-192, 2020, 646-651.
- [33] Hosseini, M., et al., Size-Dependent Stress Analysis of Single-Wall Carbon Nanotube Based on Strain Gradient Theory, *International Journal of Applied Mechanics*, 09(06), 2017, 1750087.
- [34] Pourabdy, M., et al., Analysis of Axisymmetric Vibration of Functionally-Graded Circular Nano-Plate Based on the Integral Form of the Strain Gradient Model, *Journal of Applied and Computational Mechanics*, 7(4), 2021, 2196-2220.
- [35] Jiang, Y., Li, L., Hu, Y., Strain gradient elasticity theory of polymer networks, *Acta Mechanica*, 233(8), 2022, 3213-3231.
- [36] Li, L., Hu, Y., Li, X., Longitudinal vibration of size-dependent rods via nonlocal strain gradient theory, *International Journal of Mechanical Sciences*, 115-116, 2016, 135-144.
- [37] Li, L., Li, X., Hu, Y., Free vibration analysis of nonlocal strain gradient beams made of functionally graded material, *International Journal of Engineering Science*, 102, 2016, 77-92.
- [38] Attia, M.A., Rahman, A.A.A., On vibrations of functionally graded viscoelastic nanobeams with surface effects, *International Journal of Engineering Science*, 127, 2018, 1-32.
- [39] Esfahani, S., Khadem, S.E., Mamaghani, A.E., Nonlinear vibration analysis of an electrostatic functionally graded nano-resonator with surface effects based on nonlocal strain gradient theory, *International Journal of Mechanical Sciences*, 151, 2019, 508-522.
- [40] Hashemian, M., Foroutan, S., Toghraie, D., Comprehensive beam models for buckling and bending behavior of simple nanobeam based on nonlocal strain gradient theory and surface effects, *Mechanics of Materials*, 139, 2019, 103209.
- [41] Lu, L., Guo, X., Zhao, J., A unified size-dependent plate model based on nonlocal strain gradient theory including surface effects, *Applied Mathematical Modelling*, 68, 2019, 583-602.
- [42] Zhou, S., et al., Free vibration analysis of bilayered circular micro-plate including surface effects, *Applied Mathematical Modelling*, 70, 2019, 54-66.
- [43] Ghorbani, K., et al., Investigation of surface effects on the natural frequency of a functionally graded cylindrical nanoshell based on nonlocal strain gradient theory, *The European Physical Journal Plus*, 135(9), 2020, 1-23.
- [44] Hamidi, B.A., Hosseini, S.A., Hayati, H., Forced torsional vibration of nanobeam via nonlocal strain gradient theory and surface energy effects under moving harmonic torque, *Waves in Random and Complex Media*, 32, 2022, 318-333.
- [45] Malikan, M., Eremeyev, V.A., Post-critical buckling of truncated conical carbon nanotubes considering surface effects embedding in a nonlinear Winkler substrate using the Rayleigh-Ritz method, *Materials Research Express*, 7(2), 2020, 025005.
- [46] Li, Z., et al., A standard experimental method for determining the material length scale based on modified couple stress theory, *International Journal of Mechanical Sciences*, 141, 2018, 198-205.
- [47] Thanh, C.-L., Ferreira, A., Wahab, M.A., A refined size-dependent couple stress theory for laminated composite micro-plates using isogeometric analysis, *Thin-Walled Structures*, 145, 2019, 106427.
- [48] Thanh, C.-L., et al., The size-dependent thermal bending and buckling analyses of composite laminate microplate based on new modified couple stress theory and isogeometric analysis, *Computer Methods in Applied Mechanics and Engineering*, 350, 2019, 337-361.
- [49] Babaei, H., Eslami, M.R., Size-dependent vibrations of thermally pre/post-buckled FG porous micro-tubes based on modified couple stress theory, *International Journal of Mechanical Sciences*, 180, 2020, 105694.
- [50] Najafzadeh, M., et al., Torsional vibration of the porous nanotube with an arbitrary cross-section based on couple stress theory under magnetic field, *Mechanics Based Design of Structures and Machines*, 50, 2022, 726-740.
- [51] Thai, C.H., et al., A size-dependent quasi-3D isogeometric model for functionally graded graphene platelet-reinforced composite microplates based on the modified couple stress theory, *Composite Structures*, 234, 2020, 111695.
- [52] Al-Furjan, M., et al., Vibrational characteristics of a higher-order laminated composite viscoelastic annular microplate via modified couple stress theory, *Composite Structures*, 257, 2021, 113152.
- [53] Ebrahimian, M.R., et al., Nonlinear coupled torsional-radial vibration of single-walled carbon nanotubes using numerical methods, *Journal of Computational Applied Mechanics*, 52(4), 2021, 642-663.
- [54] Eltahir, M.A., Mohamed, N., Mohamed, S.A., Nonlinear buckling and free vibration of curved CNTs by doublet mechanics, *Smart Structures and Systems, An International Journal*, 26(2), 2020, 213-226.
- [55] Eltahir, M., Abdelrahman, A.A., Esen, I., Dynamic analysis of nanoscale Timoshenko CNTs based on doublet mechanics under moving load, *The European Physical Journal Plus*, 136(7), 2021, 1-21.
- [56] Romano, G., Barretta, R., Stress-driven versus strain-driven nonlocal integral model for elastic nano-beams, *Composites Part B: Engineering*, 114, 2017, 184-188.
- [57] Eringen, A.C., Linear theory of nonlocal elasticity and dispersion of plane waves, *International Journal of Engineering Science*, 10(5), 1972, 425-435.
- [58] Eringen, A.C., On differential equations of nonlocal elasticity and solutions of screw dislocation and surface waves, *Journal of Applied Physics*, 54(9), 1983, 4703-4710.
- [59] Shishesaz, M., et al., Nonlinear Vibration Analysis of Nano-Disks Based on Nonlocal Elasticity Theory Using Homotopy Perturbation Method, *International Journal of Applied Mechanics*, 11(02), 2019, 1950011.
- [60] Shishesaz, M., Shariati, M., Yaghootian, A., Nonlocal Elasticity Effect on Linear Vibration of Nano-circular Plate Using Adomian Decomposition Method, *Journal of Applied and Computational Mechanics*, 6(1), 2020, 63-76.
- [61] Shariati, M., et al., Nonlocal effect on the axisymmetric nonlinear vibrational response of nano-disks using variational iteration method, *Journal of Computational Applied Mechanics*, 52(3), 2021, 507-534.
- [62] Rafii-Tabar, H., Ghavanloo, E., Fazelzadeh, S.A., Nonlocal continuum-based modeling of mechanical characteristics of nanoscopic structures, *Physics Reports*, 638, 2016, 1-97.
- [63] Romano, G., et al., Constitutive boundary conditions and paradoxes in nonlocal elastic nanobeams, *International Journal of Mechanical Sciences*, 121, 2017, 151-156.
- [64] Apuzzo, A., et al., Novel local/nonlocal formulation of the stress-driven model through closed form solution for higher vibrations modes, *Composite Structures*, 252, 2020, 112688.
- [65] Darban, H., et al., Size-dependent buckling analysis of nanobeams resting on two-parameter elastic foundation through stress-driven nonlocal elasticity model, *Mechanics of Advanced Materials and Structures*, 28, 2021, 2408-2416.
- [66] Luciano, R., et al., Variational approaches for bending and buckling of non-local stress-driven Timoshenko nano-beams for smart materials, *Mechanics Research Communications*, 103, 2020, 103470.
- [67] Zhang, P., Qing, H., Gao, C.F., Exact solutions for bending of Timoshenko curved nanobeams made of functionally graded materials based on stress-driven nonlocal integral model, *Composite Structures*, 245, 2020, 112362.
- [68] Penna, R., et al., Nonlinear free vibrations analysis of geometrically imperfect FG nano-beams based on stress-driven nonlocal elasticity with initial pretension force, *Composite Structures*, 255, 2021, 112856.
- [69] Roghani, M., Rouhi, H., Nonlinear stress-driven nonlocal formulation of Timoshenko beams made of FGMs, *Continuum Mechanics and Thermodynamics*, 33(2), 2021, 343-355.



- [70] Shariati, M., et al., A review on stress-driven nonlocal elasticity theory, *Journal of Computational Applied Mechanics*, 52(3), 2021, 535-552.
- [71] Shariati, M., et al., On the calibration of size parameters related to non-classical continuum theories using molecular dynamics simulations, *International Journal of Engineering Science*, 168, 2021, 103544.
- [72] Shishesaz, M., Shariati, M., Hosseini, M., Size-Effect Analysis on Vibrational Response of Functionally Graded Annular Nano-Plate Based on Nonlocal Stress-Driven Method, *International Journal of Structural Stability and Dynamics*, 22(09), 2022, 2250098.
- [73] Shariati, M., et al., Size Effect on the Axisymmetric Vibrational Response of Functionally Graded Circular Nano-Plate Based on the Nonlocal Stress-Driven Method, *Journal of Applied and Computational Mechanics*, 8(3), 2022, 962-980.
- [74] Reddy, J.N., *Mechanics of laminated composite plates and shells: theory and analysis*, CRC press, 2003.
- [75] Irie, T., Yamada, G., Takagi, K., Natural frequencies of thick annular plates, *Journal of Applied Mechanics*, 49(3), 1982, 633-638.
- [76] Shishesaz, M., Shariati, M., Hosseini, M., Size-Effect Analysis on Vibrational Response of Functionally Graded Annular Nano-Plate Based on Nonlocal Stress-Driven Method, *International Journal of Structural Stability and Dynamics*, 22(09), 2022, 2250098.
- [77] Wu, T.Y., Liu, G.R., Application of generalized differential quadrature rule to sixth-order differential equations, *Communications in Numerical Methods in Engineering*, 16(11), 2000, 777-784.
- [78] Shu, C., Richards, B.E., Application of generalized differential quadrature to solve two-dimensional incompressible Navier-Stokes equations, *International Journal for Numerical Methods in Fluids*, 15(7), 1992, 791-798.
- [79] Quan, J.R., Chang, C.T., New insights in solving distributed system equations by the quadrature method—I. Analysis, *Computers & Chemical Engineering*, 13(7), 1989, 779-788.
- [80] Kang, K., Bert, C.W., Striz, A.G., Vibration analysis of shear deformable circular arches by the differential quadrature method, *Journal of Sound and Vibration*, 183(2), 1995, 353-360.
- [81] Wu, T.Y., Liu, G.R., The generalized differential quadrature rule for fourth-order differential equations, *International Journal for Numerical Methods in Engineering*, 50(8), 2001, 1907-1929.
- [82] Han, J.B., Liew, K.M., Axisymmetric free vibration of thick annular plates, *International Journal of Mechanical Sciences*, 41(9), 1999, 1089-1109.

ORCID iD

Mojtaba Shariati  <https://orcid.org/0000-0002-7032-548X>

Mohammad Shishesaz  <https://orcid.org/0000-0002-1892-1946>

Reza Mosalmani  <https://orcid.org/0000-0002-8036-9638>



© 2022 Shahid Chamran University of Ahvaz, Ahvaz, Iran. This article is an open access article distributed under the terms and conditions of the Creative Commons Attribution-NonCommercial 4.0 International (CC BY-NC 4.0 license) (<http://creativecommons.org/licenses/by-nc/4.0/>).

How to cite this article: Shariati M., Shishesaz M., Mosalmani R. Stress-driven Approach to Vibrational Analysis of FGM Annular Nano-plate based on First-order Shear Deformation Plate Theory, *J. Appl. Comput. Mech.*, 9(3), 2023, 637-655. <https://doi.org/10.22055/jacm.2022.41125.3704>

Publisher's Note Shahid Chamran University of Ahvaz remains neutral with regard to jurisdictional claims in published maps and institutional affiliations.

